論文 / 著書情報
Article / Book Information

題目(和文)	脱ユビキチン化酵素USP8およびSTAMBPL1の活性制御機構およびその生理的病理的意義の解明
Title(English)	Cis-regulations of USP8 and STAMBPL1 deubiquitinases and their pathophysiological roles
著者(和文)	柿原慧遵
Author(English)	Keijun Kakihara
出典(和文)	学位:博士(理学), 学位授与機関:東京工業大学, 報告番号:甲第12335号, 授与年月日:2023年3月26日, 学位の種別:課程博士, 審査員:藤田 尚信,木村 宏,北口 哲也,中村 信大,加藤 明,駒田 雅之
Citation(English)	Degree:Doctor (Science), Conferring organization: Tokyo Institute of Technology, Report number:甲第12335号, Conferred date:2023/3/26, Degree Type:Course doctor, Examiner:,,,,,
学位種別(和文)	博士論文
Type(English)	Doctoral Thesis

(2022 Doctoral Thesis)

Cis-regulations of USP8 and STAMBPL1 deubiquitinases and their pathophysiological roles

脱ユビキチン化酵素 USP8 および STAMBPL1 の活性制御機構およびその生理的病理的意義の解明

Department of Life Science and Technology,
Tokyo Institute of Technology

Keijun Kakihara
(Supervisor: Associate Prof. Naonobu Fujita)

東京工業大学
生命理工学院

柿原慧遵
（指導教員　藤田尚信　准教授）

Abstract

Protein ubiquitination is a reversible modification; it is balanced via ubiquitination and deubiquitination reactions. The latter is catalyzed by deubiquitinases (DUBs). DUBs regulate various cellular functions and are associated with many human diseases. Most DUBs are multi-domain proteins, including catalytic and regulatory domains; however, little is known about the regulatory mechanisms of DUB activation and their pathophysiological roles. To elucidate these issues, I studied two DUBs, ubiquitin-specific protease 8 (USP8) and STAM-binding protein-like 1 (STAMBPL1). For USP8, I identified an autoinhibitory WW-like domain that interacts with and inhibits the catalytic domain. Cushing's disease-associated mutations of USP8 reduced the interaction between the WW-like and catalytic domains, over-activating USP8 and likely leading to the onset of the disease. For STAMBPL1, I determined an autoinhibitory MIT domain that interacts with the catalytic domain. I also found that, upon apoptosis induction, STAMBPL1 activated through cleavage-dependent removal of the MIT domain, being involved in apoptosis progression. Together, this study showed the autoinhibitory mechanisms of USP8 and STAMBPL1 and their pathophysiological roles.

Index

1. General introduction

1.1 Ubiquitination: function, modality and “ubiquitin code”

Protein ubiquitination is a post-translational modification (PTM) to target various intracellular proteins to degradation, localization, complexation, activation, and other destinies. Ubiquitination regulates various cellular functions, including proteostasis, membrane trafficking, signal transduction, and DNA repair.

In this modification, the C-terminus of ubiquitin protein is covalently conjugated to the amino group of the side chain of a lysine residue (or the N-terminal amino group of the first methionine) of the target protein. Ubiquitin has seven lysine and the first methionine residues. The ubiquitin conjugated to the target can be utilized as an acceptor site for the next ubiquitin, forming a polyubiquitin chain. Ubiquitination modality on the target protein can be structurally classified as monoubiquitin, multi-monoubiquitin, homotypic polyubiquitin chain (Met1, Lys6, Lys11, Lys27, Lys29, Lys33, Lys48, and Lys63-linkages), and heterotypic polyubiquitin chains (mixed and branched-linkages) (Komander et al., 2012) (Fig. 1a, left and middle).

Different types of ubiquitination can target substrate proteins to distinct destinies (Swatek et al., 2016). For example, the Lys48-linked ubiquitin chain induces proteasomal degradation, and the Lys63-linked ubiquitin chain regulates their trafficking. This “ubiquitin code” system may be based on the interactions between each type of ubiquitin moiety and their specific binding proteins (i.e., decoder proteins), but the underlying mechanisms remain unclear. Furthermore, recent reports uncover novel ubiquitination modalities (Swatek et al., 2016; Dikic et al., 2022). They include new ubiquitination targets (serine, threonine, and cysteine residues; sugar; lipid) and the modification of ubiquitin (phosphorylation and acetylation) (Fig. 1a, right). Therefore, understanding the whole picture of ubiquitin code became further complicated and mysterious.

1.2 Deubiquitinase families and their substrate specificity

Ubiquitination is reversible; it is balanced via ubiquitination and deubiquitination. The latter reaction is catalyzed by deubiquitinases (DUBs). The human genome encodes around 100 DUBs, including seven families with different catalytic domains (Mevissen et al., 2017) (Fig. 1b). Six of them are cysteine-based protease families; ubiquitin-specific proteases (USPs), ovarian tumor proteases (OTUs), ubiquitin C-terminal hydrolases

(UCHs), Machado-Josephin domain proteases (MJDs), motif interacting with ubiquitin-containing novel DUB family (MINDYs), and a zin-finger-containing ubiquitin peptidase (ZUP). The other is a zinc-binding metalloprotease family, the Jab1/Mov34/MPN+ proteases (JAMMs).

Recent proteomic analysis of human cells identified ~10,000 ubiquitinated proteins and ~100,000 ubiquitinated sites (Vere et al., 2020). Human E3 ubiquitin ligases are predicted to be encoded by ~1,000 genes (Zheng et al., 2017). These suggest that each DUB should catalyze a variety of intracellular proteins. However, no single DUB would catalyze all ubiquitinated proteins. Knockout or knockdown of a single DUB gene often causes phenotypic changes in cells and mice, showing that most DUBs have a unique function for which other members cannot compensate.

Substrate specificity of DUBs is determined by their gene expression, intracellular localization, and substrate recognition by the protein-protein interaction through intrinsic domain or adaptor proteins. In addition, some DUBs deubiquitinate specific ubiquitin linkages by recognizing them with ubiquitin-interacting motifs (UIMs) and ubiquitin-binding domains, including their catalytic domain (Clague et al., 2019). For example, OTU domain-containing deubiquitinase with linear linkage specificity (OTULIN) is strictly specific for the Met1-linked ubiquitin chain. A USP CYLD specifically cleave Met1- and Lys63-linked chains. USP30 prefers Lys6-linked chain. USP25 utilizes its intrinsic tandem UIMs to prefer Lys48-linked ubiquitin chain (Kawaguchi et al., 2017). Further, some DUBs recognize ubiquitin chain length to perform their full catalytic activity. They even prefer whether they cleave the ubiquitin chain from the distal end (exo-cleavage) or within chains (endo-cleavage). For example, MINDY-1/2 sense the length of the Lys48-linked chain and switch exo- and endo-cleavage activity depending on the chain length (Abdul Rehman et al., 2021). Overall, while the underlying structural bases are not fully understood, some DUBs deubiquitinate substrates in a chain type- and length-dependent manner and prefer exo- and endo-cleavage.

1.3 Regulation of DUB activity

Enzymatic activities of DUBs are often regulated via their PTMs and interaction with regulatory proteins (Fig. 1c). For example, CYLD requires phosphorylation at the proximate site to the catalytic domain for its catalytic activity toward the Lys63-linked ubiquitin chain (Elliott et al., 2021). BRCA1/BRCA2-containing complex subunit 36

(BRCC36), a member of JAMMs, in dimeric BRCC36 isopeptidase complex (BRISC) is inhibited via interaction with dimeric serine hydroxymethyltransferase 2 (SHMT2) but not tetrameric SHMT2 (Rabl et al., 2019; Walden et al., 2019). USP25 is active in the dimeric state, whereas inactive in the tetrameric state, because USP25 inhibits its activity via their intermolecular interaction (Gersch et al., 2019; Sauer et al., 2019). Most DUBs are multi-domain proteins harboring uncharacterized domains. Furthermore, some catalytic domains have large insert sequences dispensable for the catalytic reaction (Ye et al., 2009). These facts raise a possibility that these domains/sequences are involved in their activity regulation. However, the cis-regulation of DUBs and the underlying mechanisms are largely unknown. Researchers are trying to challenge these issues.

1.4 DUBs and human diseases

Many DUBs are involved in the pathogenic mechanisms of various human diseases, sometimes accompanied by their aberrant expression levels. For example, the high expression level of STAM binding protein-like 1 (STAMBPL1) is related to some cancers (Chen et al., 2019; Shahriyar et al., 2018; Yu et al., 2019). USP16 and USP25 gene triplication are associated with the onset of down syndrome and its complicated Alzheimer's syndrome (Adorno et al., 2013; Zheng et al., 2021). Loss-of-function and gain-of-function mutations in DUBs are also related to multiple cancers, developmental disorders, and syndromes (Table. 1). For example, loss-of-function mutations of CYLD and OTULIN, two DUBs regulating innate immune signaling, cause multiple tumors of the skin appendages (cylindromatosis) and OTULIN-related autoinflammatory syndrome, respectively (Damgaard et al., 2016; Zhou et al., 2016). Loss-of-function mutations of BRCA1-associated protein 1 (BAP1) are related to renal cell carcinoma (Harbour et al., 2010; Peña-Llopis et al., 2012). Loss-of-function mutations of STAMBP are frequently found in microcephaly-capillary malformation (MIC-CAP) syndrome (McDonell et al., 2013). On the other hand, gain-of-function mutations in USP8 and USP48 are identified as pathogenetic factors of Cushing's disease (Reincke et al., 2015; Chen et al., 2018).

1.5 Aim of this study

In this study, I focused on two endosomal DUBs, USP8 and STAMBPL1, and revealed their cis-regulations. My structural analysis illuminated that, in both cases, their intrinsic domain interacts with and blocks the ubiquitin-binding site in the catalytic domain, thus

autoinhibiting their activity. I also show the relief of their autoinhibition by intracellular signaling and disease-associated mutations, highlighting the physiological and pathological significance of their cis-regulation systems.

2. Chapter 1　Molecular basis of USP8 autoinhibition by its WW-like domain and the dysregulation in Cushing's disease.

2.1 Introduction

USP8, a member of USP family DUBs, plays roles in various cellular events, especially membrane trafficking pathways such as endocytosis. USP8 regulates ubiquitinated-cargo sorting system on the endosome. USP8 deubiquitinates these cargo proteins including epidermal growth factor receptor at the early endosomes, thereby preventing their ubiquitin-dependent lysosomal degradation and enhancing their recycling to the plasma membrane (Le Clorennec et al., 2016; Li et al., 2012; Ma et al., 2016; Mizuno et al., 2005; Mukai et al., 2010; Niendorf et al., 2007; Oh et al., 2014; Xia et al., 2012).

USP8 is a multi-domain protein including its catalytic USP domain. The USP domain in USP8 comprises three subdomains, the fingers, palm and thumb (Fig. 2a) (Clague et al., 2019; Ye et al., 2009). These subdomains cooperatively form the ubiquitin-binding pocket, which recognizes the globular core of the distal ubiquitin. A deep cleft between the palm and the thumb subdomains functions as a catalytic cleft, at which the catalytic triad (Cys, His and Asp/Asn residues) attacks the isopeptide bond between the distal ubiquitin C-terminal tail and proximal ubiquitin (or substrate protein). Moreover, two loops surrounding the catalytic cleft, namely blocking loops 1 and 2 (BL1 and BL2), are predicted to be involved in ubiquitin recognition (Avvakumov et al., 2006). USP8 can deubiquitinate all types of polyubiquitin chain in vitro.

In our previous study, a C-terminal USP8 fragment consisting only of the USP domain showed increased activity (Reincke et al., 2015), suggesting that USP8 harbors an autoinhibitory region. Our laboratory member Asamizu generated a series of USP8 deletion constructs (Fig. 2b) and evaluated their activities toward Lys63-linked ubiquitin tetramers in vitro. The results indicate that a middle region (aa. 645-684) in USP8 autoinhibits USP8 activity (Fig. 2c).

To confirm the effects of the autoinhibitory region on ubiquitin-binding ability of USP8, Asamizu also tested the labeling efficiency of wild-type USP8 ($USP8^{WT}$) or the truncated mutant lacking the aa 645-684 ($USP8^{\Delta 645\text{-}684}$) with ubiquitin-vinyl methyl ester (Ub-VME), which can be irreversibly conjugated to the catalytic core of USP domain (Borodovsky et al., 2002). $USP8^{\Delta 645\text{-}684}$ was labeled by Ub-VME more effectively than

USP8^{WT} (Fig. 2d), implying that the autoinhibitory region hinders ubiquitin recognition by the USP domain.

An amino acid sequence of the autoinhibitory region is well conserved among vertebrates (Fig. 2e) and shows sequence similarity to MAGI1 WW domain (aa. 359-392) (Fig. 2f). Typical WW domains have two conserved tryptophan residues (Salah et al., 2012). However, some WW domains in MAGI1, SAV1 and WWOX only have the first one (Fig. 2f), although these atypical WW domains show similar conformation to typical WW domains (Ohnishi et al., 2008). The autoinhibitory region of USP8 also only has the first tryptophan residue (Trp655), sharing a common feature of atypical WW domains. Asamizu thus named this autoinhibitory region in USP8 as a WW-like domain. Together, he concluded that the WW-like domain inhibits ubiquitin recognition by the USP domain, autoinhibiting USP8 activity (Asamizu., 2018, Master thesis). However, the molecular mechanism underlying the autoinhibition is yet understood.

USP8 activity is also regulated by 14-3-3 proteins which bind to the 14-3-3-binding motif in USP8 in a phospho-dependent manner. This 14-3-3-binding suppresses USP8 activity (Mizuno et al., 2007). In the mitotic M-phase, USP8 dissociates from 14-3-3 proteins and becomes enzymatically active (Mizuno et al., 2007). On the other hand, in corticotroph adenomas of Cushing's disease, ~50% of tumor samples show somatic mutations of USP8 gene, that cause deletion or substitution of amino acids around the 14-3-3-binding motif (Ma et al., 2015; Reincke et al., 2015). Importantly, these mutations in the 14-3-3-binding motifs increase USP8 activity. In addition, a recent paper reports a somatic mutation located at the middle region other than the 14-3-3-binding motif, the substitution of Gly664 to Arg (Treppiedi et al., 2021). Cushing's disease begins with the hypersecretion of adrenocorticotropic hormone (ACTH) from corticotrophs, followed by excess adrenal glucocorticoid. In cultured corticotrophs, the exogenous expression of these disease-associated USP8 mutants effectively enhances ACTH secretion (Reincke et al., 2015), suggesting that USP8 over-activation causes this disease. However, the molecular basis of 14-3-3-dependent inhibition of USP8 activity remains unclear.

This study aimed to elucidate the molecular mechanism underlying USP8 over-activation by Cushing's disease-associated mutations.

2.2 Materials and Methods

cDNA preparation and plasmid construction

Human USP8 cDNA (Reincke et al., 2015), human 14-3-3ε cDNA (Mizuno et al., 2007), mouse STAM1 cDNA (Mizuno et al., 2003), and mouse STAM2 cDNA (Takata et al., 2000) were prepared elsewhere. Human Parkin cDNA and human ubiquitin cDNA were kindly donated by Dr. Koji Yamano and Dr. Toshiaki Suzuki, respectively (Tokyo Metropolitan Institute of Medical Science, Japan). For the construction of expression plasmids, these cDNAs were subcloned into the following vectors; pME (Reincke et al., 2015) for the expression of C-terminal FLAG-tagged USP8; pCDH-CMV-MCS-EF1-Puro (System Biosciences) for the viral infection and expression of N-terminal FLAG-tagged USP8; pcDNA3 (Invitrogen) for N-terminal HA-tagged USP8; pFLAG-CMV2 (Sigma Aldrich) for N-terminal FLAG-tagged USP8, Parkin, STAM1, and STAM2; pmyc-CMV5 (gift from Dr. Jun Nakae, Keio University, Tokyo, Japan) for N-terminal myc-tagged USP8 and 14-3-3ε; pGEX-6P2 (GE Healthcare) for the bacterial expression of N-terminal GST-tagged USP domain (aa. 756-1118); pGEX-6P1 (GE Healthcare) for the bacterial expression of N-terminal GST-tagged USP8 constructs (aa. 645-1110 or 756-1110). For construction of single molecule FRET probes, human USP8 (aa 645-684) was subcloned into pEYFP-N1 (Clonetech). ECFP with flexible spacers consisting of 10 aa peptide (-Gly-Gly-Ser-Ala-Gly-Gly-Ser-Ala-Gly-Gly-) was amplified by PCR from pECFP-N1 (Clonetech) (Komatsu et al., 2011; Levskaya et al., 2009). For ECFP insertion, restriction sites for EcoRI and BamHI were inserted in the following points of USP domain; a gap between aa 816/817 as insert-1; aa 898/899 as insert-2 (FRIP8); aa 959/960 as insert-3; aa 1045/1046 as insert-4; aa 1074/1075 as insert-5 (Ye et al., 2009). ECFP with the spacers was stepwise subcloned into these EcoRI and BamHI sites. Site-specific mutagenesis was performed by PCR using Prime STAR mutagenesis basal kit (Takara).

Protein preparation

GST-tagged USP domain (aa. 756-1118) or GST-tagged USP8 constructs (aa. 645-1110 or 756-1110) were produced in *E.coli* Rosetta (DE3) pLysS cells. Protein expression was induced by the stimulation of cells with 0.5 mM IPTG, followed by overnight culture at 15 or 18 ℃, respectively. Cells were then lysed in ice-cold PBS supplemented with 1 % Triton X-100 and protease inhibitors (1 μg/ml aprotinin, 1 μg/ml leupeptin and 1 μg/ml pepstatin A). After centrifugation, the supernatants were mixed with Glutathione Sepharose 4B (GE Healthcare). For GST-tagged USP domain,

after 1 h incubation at 4 ˚C, beads were washed five times with PBS, and then incubated in ice-cold elution buffer A (50 mM Tris-HCl pH 8.0, 1 mM EDTA, 1mM DTT, and 10 mM reduced glutathione (Wako)) at 4 ˚C for 30 min. For GST-tagged USP8 constructs, after 1 h incubation at 4 ˚C, beads were washed five times with PBS, and then incubated with prescission protease (Cytiva) following the manufacture's protocol. The purity and concentration of eluates were validated by SDS-PAGE and CBB staining using Quick CBB (Wako).

His-tagged FRIP8 were expressed in HEK293T cells. Cell culture and transfection are described below. Cells were lysed in ice-cold lysis buffer (50 mM Tris-HCl pH 7.4, 150 mM NaCl, 50 mM NaF, 1 % Triton-X-100) supplemented with 10 mM imidazole and protease inhibitors. After centrifugation, the supernatants were mixed with Ni-NTA agarose beads (QIAGEN). After 2 h incubation at 4 ˚C, beads were washed five times with Tris buffered saline (TBS) (20 mM Tris-HCl pH 7.4, and 150 mM NaCl), and then incubated in ice-cold elution buffer B (20 mM Tris-HCl pH 7.4, 150 mM NaCl, and 250 mM imidazole) at 4 ˚C for 30 min. The purity was validated using immunoblotting.

For *in vitro* deubiquitination (DUB) assay, FLAG-tagged USP8 (wild-type and mutants) were expressed in HEK293 cells or HEK293T cells. Cell lysis and immunoprecipitation were carried out as described below. USP8 levels in each sample were compared by immunoblotting, and equal number of USP8 molecules were subjected to the assay.

Cell culture, plasmid transfection and lentivirus infection

HEK293 cells, HEK293T cells, and HeLa cells were grown in Dulbecco's modified Eagle's medium (DMEM) (Nacalai Tesque) supplemented with 10 % fetal bovine serum (FBS), 100 units/ml penicillin, and 0.1 mg/ml streptomycin at 37 °C and 5 % CO_2. To stimulate cells with EGF, the cells were cultured in the presence of 0.5 % FBS for the last 24 h, and then incubated with 100 ng/ml human EGF (PeproTech) at 37 ˚C for 5 min.

Plasmids transfection was carried out using polyethyleneimine (Polyscience) according to the standard protocol. Cells were subjected to analyses 24-48 h after transfection.

For lentivirus production, HEK293T cells were transfected with pCDH-CMV-FLAG-USP8-EF1-Puro, psPAX2 (Addgene #12260), and pCMV-VSV-G (Addgene #8454). Two days after transfection, the medium containing the virus was collected and

filtrated. HeLa cells were infected by the virus medium in the presence of 8 μg/ml polybrene (Nacalai Tesque). From 2 days after infection, cells were cultured in the presence of 0.8 μg/ml puromycin. Survived cells were used for experiments.

Cell lysis, immunoprecipitation and immunoblotting

Cells were lysed with ice-cold lysis buffer (50 mM Tris-HCl pH 7.4, 150 mM NaCl, 50 mM NaF, 1 % Triton-X-100) supplemented with protein inhibitors. For the detections of the ubiquitin signals by immunoblotting, 2 mM N-ethylmaleimide (Sigma Aldrich) was added. For the cell lysis or immunoprecipitation of FLAG-tagged USP8 for DUB assay, 1 mM DTT (Nacalai Tesque) was added. After centrifugation of lysates, the supernatants were collected. To examine effects of R18 peptide (Sigma Aldrich) on the interaction of 14-3-3 and USP8 or FRIP8, the lysates were incubated with R18 peptide at 4 ℃ for 30 min.

Immunoprecipitation was performed using standard procedures. Anti-FLAG M2 antibody-conjugated agarose beads (Sigma Aldrich), anti-EGFR antibody (#MI-12-1, MBL), anti-GFP antibody (#M-048-3, MBL), and Protein A-Sepharose (GE Healthcare) were used for immunoprecipitation. After immunoprecipitation, beads were washed five times with lysis buffer. For the elution of FLAG-tagged proteins, beads were incubated in TBS with 200 ng/μl FLAG peptide (Sigma Aldrich) at 4 ℃ for 30 min.

Samples were incubated in SDS-PAGE sample buffer (62.5 mM Tris-HCl pH 6.8, 2 % SDS, 5 % 2-mercapto ethanol, 10 % glycerol, and 0.1 mg/ml bromo phenol blue) at 98 ℃ for 5 min. Otherwise, for the detections of the ubiquitin signals, samples were incubated in NuPAGE LDS sample buffer with reducing agent (Thermo Scientific) at 37 ℃ for 20 min. Samples were separated by SDS-PAGE or NuPAGE (Thermo Scientific).

Immunoblotting were performed using standard procedures. Primary antibodies for immunoblotting were as follows: anti-FLAG antibody (clone 1E6, Wako), anti-Ubiquitin (#D058-3, MBL; #3936, Cell Signaling), anti-EGFR antibody (#MI-12-1, MBL), anti-USP8 antibody (Kato et al., 2000), anti-HRS antibody (Komada and Kitamura, 1995), anti-STAM1 antibody (Mizuno et al., 2004), anti-α-tubulin antibody (clone 10G10, Wako), anti-HA antibody (clone 3F10, Sigma Aldrich; #SC-57592, Santa Cruz), anti-Myc antibody (#SC-40, Santa Cruz; clone 9E10, hybridoma supernatant), anti-GFP antibody (#A-11122, Thermo Scientific), and anti-14-3-3 antibody (#SC-1657, Santa

Cruz). Secondary antibodies were peroxidase-conjugated anti-mouse IgG, anti-rat IgG, and anti-rabbit IgG antibodies (GE Healthcare). Blots were detected using ECL Prime Western Blotting Detection Reagents (GE Healthcare) and ImageQuant LAS 4000mini (GE Healthcare).

Quantitative DUB assay

For ubiquitin chain cleavage assay, FLAG-tagged USP8 (wild-type or the mutants) was incubated with 25 ng/μl Lys63-linked ubiquitin tetramers (Boston Biochem) in TBS with 10 mM dithiothreitol at 37 ˚C for indicated time, in the presence or absence of R18 peptide. Samples were subjected to SDS-PAGE or NuPAGE, followed by gels staining with Silver Stain MS kit (Wako).

For ubiquitin-AMC assay using FLAG-tagged USP8, FLAG-tagged USP8 was mixed with 1 μM ubiquitin-AMC (Boston Biochem) and 10 mM DTT in TBS, in 96 well medium-binding, flat bottom, black plates (Thermo Scientific). For ubiquitin-AMC assay using GST-tagged USP8 constructs, 100 nM GST-tagged USP8 constructs were mixed with 10 mM DTT in TBS and incubated at 37 ˚C for 10 min. Subsequently, samples were mixed with 1 μM ubiquitin-AMC (Boston Biochem) in 384 well FLUOTRAC 200 plate (Greiner). Plates were set on Varioskan LUX (Thermo Scientific), and incubated at 37 ˚C. During the incubation, fluorescence intensity of AMC released from ubiquitin was measured at 10 or 30 sec intervals using 345 nm and 445 nm as excitation wavelength and emission wavelength, respectively. The fluorescence intensity of the sample without USP8 was measured as background and subtracted from each value. The non-linear regression curves were plotted using the equation for one-phase association by Prism 9 (GraphPad Software).

Ubiquitin labeling assay

For ubiquitin-conjugated vinyl methyl ester (Ub-VME) labeling, FLAG-tagged USP8 immunoprecipitates or His-tagged FRIP8 precipitates were incubated with 1 μM Ub-VME (Boston Biochem) in TBS supplemented with 1 mM DTT at 37 °C for 5 min or 30 min, respectively.

For HA-tagged ubiquitin-conjugated vinyl sulfone (HA-Ub-VS) labeling, the lysate of HEK293 cells expressing FLAG-tagged USP8 were supplemented with 1 mM DTT, incubated with 1 μM HA-Ub-VS (Boston Biochem) at 37 °C for 30 min, and subjected

to immunoprecipitation using monoclonal anti-HA-agarose antibody (Sigma Aldrich) at 4 °C for 60 min. Samples were subsequently subjected to immunoblotting and FRET assay.

Amino acid sequence alignment

Protein BLAST (https://blast.ncbi.nlm.nih.gov/) was used to find protein sequences similar to USP8 aa 645-684. Sequence similarity was analyzed by ClustalW program (https://clustalw.ddbj.nig.ac.jp/). The colors in the alignment follow ClustalX scheme. Amino acid sequences of human MAGI1 (Accession code: Q96QZ7), human SAV1 (Q9H4B6), human WWOX (Q9NZC7), and vertebrate USP8s were based on annotated information in uniprot database (https://www.uniprot.org/).

***In silico* structural modeling**

In silico structural modeling of the WW-like domain, the USP domain, and their complex were performed. Briefly, (1) the homology modeling of the WW-like domain was firstly carried out using MAGI1 WW domain (PDB ID: 2YSE), (2) the structural model of the USP domain in the ubiquitin-bound form was then constructed using the ubiquitin-bound USP2 USP domain (PDB ID: 2HD5) as the template of the homology modeling, and (3) the protein-protein docking simulations of the two domains were executed by ClusPro (https://cluspro.org/). The MD simulations of the derived modeled structures were also carried out to examine their stabilities in the physiological condition. By use of the sequence similarity with MAGI1 WW domain together with the structural data by NMR experiment (PDB ID: 2YSE), the structure of WW-like domain in USP8 (residue 645-684) was modeled by MODELLER (Sali and Blundell, 1993). To perform the MD simulation, a rectangular simulation box was constructed with a margin of 12 Å to the boundary of the simulation box, resulting in the dimension, 58 Å × 51 Å × 58 Å. The solution system contained 4139 TIP3P water molecules (Jorgensen, 1983) together with one sodium ion to neutralize the simulation system, resulting in 13045 atoms in total. AMBER ff14SB (Maier et al., 2015) was applied for the potential energy of the all-atom protein. For the zinc ion in the fingers subdomain, the Zinc AMBER force field (ZAFF) (Li et al., 2013; Peters et al., 2010) was used. The MD simulations were performed by AMBER 16 (Case et al., 2005) under constant temperature and pressure (NPT) conditions at $T = 300$ K and $P = 1$ atm using Berendsen's thermostat and barostat (Juffer et al., 1991)

at a relaxation time of 1 ps, and using the particle mesh Ewald method (Darden et al., 1993) for the electrostatic interactions. The simulation length was 1 μs, together with a 2-fs time step using constraining bonds involving hydrogen atoms via the SHAKE algorithm (Ryckaert et al., 1977). The simulation of the W655S mutant was also carried out as described above after replacing Trp655 of the wild type with Ser via MODELLER (Sali and Blundell, 1993).

The structural model of the USP domain (aa. 756-1110) was also constructed to survey the potential interaction with the WW-like domain. Since the open form with bound ubiquitin was not solved for USP8, the ubiquitin-bound USP2 USP domain (PDB ID: 2HD5) was used as the template of the homology modelling. The modelled structure of the USP8 USP domain with bound 76-residue ubiquitin was then solvated in the simulation box of the dimension, 103 Å × 84 Å × 91 Å (including 65415 atoms in total), and simulated for 1 μs as described above. The stability of the modeled ubiquitin-USP domain complex was seen in the small root mean square distribution on Cα atom resolution (Cα-RMSD) of the overall structure being < 2.6 Å from the initial simulation model. The structure of the USP domain in the last simulation trajectory time step was then used for the subsequent docking simulation with the WW-like domain. The MD simulation of apo USP domain in the closed form was also carried out by use of the crystal structure (PDB ID: 2GFO) as the initial model.

Structural basis of stable complex formation between the USP domain and the WW-like domain was then pursued by use of their docking simulation. The protein-protein docking simulation was performed using protein-protein interaction server ClusPro together with the standard parameter sets (Kozakov et al., 2017), generating putative interaction complexes. Among them, we chose six model candidates from the criteria that Phe1014 of the USP domain exists in the interface with the WW-like domain, and carried out 100-ns MD simulation for each model candidate as described above. Using the associated MD trajectories, the number of atom contacts (non-hydrogen atom pair with r < 4 Å), N_c, and binding free energy evaluated using MM-GB/SA module of AMBER 16 (Case et al., 2005), ΔG_{bind}, were calculated between the USP domain and the WW-like domain. The structure with the largest N_c and the lowest ΔG_{bind} was then selected as the most probable complex model. The additional 1-μs MD simulation of the resulting USP domain/WW-like domain complex showed that the overall Cα-RMSD is less than 3.5 Å

from the initial simulation model, indicating substantial stability of the derived complex structure in physiological condition.

Pull down assay

HEK293T cells expressing indicated prey proteins were lysed with lysis buffer supplemented with protein inhibitors. The lysates were incubated with 5 μM GST or GST-tagged USP domain at 4 ℃ for 2 h, and then incubated in the presence of Glutathione Sepharose 4B at 4 ℃ for 90 min. Beads were washed five times with lysis buffer and samples were subjected to immunoblotting.

FRET assay

Samples were put in 96 well medium-binding, flat bottom, black plates. Fluorescence intensities were measured by Varioskan LUX or F2700 (Hitachi Hightech), at 5 nm wavelength intervals using 433 nm as excitation wavelength and 460 nm to 570 nm as emission wavelength range. Negative control samples were incubated with 10 ng/μl trypsin (Thermo Scientific) at 4 ℃ for 60 min, and the fluorescence intensities were measured. In blank wells, assay buffer or lysates derived from cells not expressing FRET probes were also prepared. These fluorescence intensities were measured as background signals and subtracted. FRET ratio was calculated using a peak intensity at EYFP emission wavelength divided by a peak intensity at ECFP emission wavelength.

Immunofluorescence

HeLa cells on coverslips were fixed with PBS containing 4% paraformaldehyde, permeabilized with PBS containing 0.2% Triton X-100 and blocked with PBS containing 5% FBS. Cells were stained with mouse anti-FLAG antibody (clone M2, Sigma Aldrich, 1 μg/ml) and Alexa Fluor 488-conjugated anti-mouse IgG secondary antibody (Invitrogen) based on standard procedures. Coverslips were mounted on slides with Fluoroshield mounting medium (ImmunoBioScience). Fluorescence images were captured with a laser-scanning confocal microscope (LSM 780, Carl Zeiss). For qualitative analysis, more than fifty images in each sample were obtained and analyzed using Prism 9 (GraphPad Software).

Statistical analysis

The results shown are the mean±s.d. Data were analyzed by Student's t-test or one-way factorial analysis of variance followed by Tukey–Kramer post-hoc multiple comparison test. The significance level of $P < 0.05$ shows statistically significant.

2.3 Results

USP8 has an intrinsic WW-like domain as its autoinhibitory region

I examined the effects of the deletion of the WW-like domain ($USP8^{\Delta WW\text{-}like}$) on ubiquitination levels of USP8 substrates in cells. EGF-induced ubiquitination of EGFR, a representative USP8 substrate, was lower in HeLa cells stably expressing $USP8^{\Delta WW\text{-}like}$ compared to $USP8^{WT}$ (Fig. 3a). Asamizu examined ubiquitination of other USP8 substrates STAM1 (Row et al., 2006) and STAM2 (Niendorf et al., 2007), using HEK293T cells overexpressing $USP8^{WT}$ or $USP8^{\Delta WW\text{-}like}$ (data not shown). I further examined ubiquitination of other USP8 substrate Parkin (Durcan et al., 2014), using the similar method. Their ubiquitination levels were decreased by USP8WT overexpression, and more strongly by $USP8^{\Delta WW\text{-}like}$ overexpression (Fig. 3b). These results indicate that the WW-like domain functions as an autoinhibitory region in cells as well. This domain seems not to regulate the cellular localization of USP8 because $USP8^{\Delta WW\text{-}like}$ showed a similar staining pattern to $USP8^{WT}$ (Fig. 3c).

I and my collaborators next performed in silico homology modeling using the MAGI1 WW domain (PDB ID: 2YSE) as a template. In this model, the overall structure of the WW-like domain is similar to that of canonical WW domains; three-stranded antiparallel β-sheet (Fig. 4a, left panel) (Salah et al., 2012). Like WW domains, the β-sheet surface contains several aromatic or hydrophobic side chains (Phe658, Pro661, Phe666, Tyr668, His670, and His677) (Fig. 4a, right panel), indicating its role in protein-protein interaction. In addition, the N-terminal region, where Leu651 and Pro652 contact Trp655, forms a hook structure that is often found in WW domains (Salah et al., 2012). Molecular dynamics (MD) simulations showed the stability of the model structure and revealed that the substitution of Trp655 to Ser (W655S) abolishes one of three β-strands and induces destabilization of the domain structure (Fig. 4b). Thus, the first conserved tryptophan residue seems to underpin the folding, similar to WW domains (Salah et al., 2012). These data suggest that the WW-like domain has common features of canonical WW domains even though lacking the second Trp.

I also examined USP8 activity in that Trp655 is substituted to Ser ($USP8^{W655S}$) and found that $USP8^{W655S}$ shows higher activity toward Lys63-linked Ub chain and ubiquitin-AMC (Ub-AMC), which release AMC fluorescent substance depending on the cleavage (Dang et al., 1998), than $USP8^{WT}$ (Fig. 4c and 4d). These results suggest that Trp655 in the WW-like domain is important for its inhibitory function as well as folding.

WW-like domain interacts with USP domain

I hypothesized that the WW-like domain might interact with the USP domain. Pull-down assay indicated the interaction of USP8 N-terminal region consisting of aa. 1-714 with the USP domain. This interaction was abolished by deletion of the WW-like domain and substitution of Trp655 to Ser (Fig. 5a and 5b). These results indicate that the WW-like domain can interact with the USP domain in vitro.

I also performed a single-molecule fluorescence resonance energy transfer (FRET) assay (Fig. 5c), by constructing five FRET probes as shown in Fig. 5d. These probes consist of USP8 C-terminal region (aa. 645-1118) containing the WW-like domain and the USP domain, EYFP, and ECFP. EYFP was fused to the N-terminus of the WW-like domain. ECFP was inserted into five different surface loops of the USP domain (Fig. 5d and 5e). ECFP insertion in my probes would not disrupt the tertiary structure of the USP domain, because many USP family proteins have long insertion sequences at these surface loops (Ye et al., 2009). If the WW-like domain and the USP domain interact with each other in these probes, a fluorescent signal of EYFP in response to the excitation of ECFP can be detected.

I prepared lysates of cells expressing these probes and measured emission spectra with excitation wavelength for ECFP. After that, I trypsinized the lysates to separate EYFP and ECFP in the probes by digesting other than the fluorescent proteins, and measured their emission spectra as negative controls. The representative FRET spectra is shown in Fig. 5f. The FRET ratio showed the ratio of the emission intensity of EYFP to that of ECFP. All probes showed significant FRET signals (Fig. 5g). The expression of each probe and their trypsinization were evaluated by immunoblotting (Fig. 5h). FRET signals of insert-2 and -3 probes, where the ECFP insertion sites are close to the ubiquitin-binding pocket (Fig. 5e), were relatively higher. I called the insert-2 probe a FRET-based intramolecular interaction probe of USP8 (FRIP8) and used it hereafter. These data implied that the pocket is involved in the efficient interaction with the WW-like domain.

To confirm it, I also checked whether the FRET signal is decreased by a treatment with FRIP8 with Ub-VME. I then purified His-tagged FRIP8 and incubated it with Ub-VME. Ub-VME was conjugated to FRIP8 (Fig. 5i) and decreased the FRET signal (Fig. 5j), suggesting that the WW-like domain and ubiquitin competitively interact with the ubiquitin-binding pocket. W655S mutation in FRIP8 significantly decreased the FRET signal (Fig. 5k), indicating the importance of proper folding of the WW-like domain for the interaction with the USP domain.

A previous report indicated potential USP8 dimerization via the N-terminal MIT domain (Avvakumov et al., 2006). I found USP8 dimerization by co-immunoprecipitation of FLAG-tagged and myc-tagged USP8, but neither deletion of the WW-like nor USP domains abolished the dimerization (Fig. 5l). Thus, these domains are not required for USP8 dimerization. Given that my FRET probes lack the MIT domain, I speculate that the WW-like and USP domains intramolecularly interact in my FRET probes. It cannot be ruled out that they might intermolecularly interact in a full-length USP8 dimer.

WW-like domain plugs ubiquitin-binding pocket in USP domain

I then analyzed the interaction between the WW-like and USP domains in silico. First, I predicted the USP domain structure in the ubiquitin-bound form by homology modeling using the ubiquitin-bound USP2 USP domain (PDB ID: 2HD5) (Renatus et al., 2006) as a template. The previous study solved the crystal structure of the USP domain of USP8 in apo-form and they suggested that the USP domain might be incapable of ubiquitin-binding because of its relatively closed ubiquitin-binding pocket (Fig. 6a) (Avvakumov et al., 2006). Despite its unfavorable features for deubiquitination, this USP domain by itself showed similar catalytic efficiency to those of other USPs, implying its substrate-induced conformational change. Unlike this apo-form, the predicted structure shows an open conformation, where the USP domain grabs ubiquitin molecule with the tip of the fingers and the catalytic cleft (Fig. 6b). Lys913 and Leu917 in a unique α9 helix (aa. 902-918) also physically contact with ubiquitin. The C-terminal tail of ubiquitin is embedded in the catalytic cleft, supported by BL1 and BL2. The catalytic triad keeps aligned in an active form in the model.

Next, I tried to identify the putative binding site(s) by examining the effects of point mutations in FRIP8 on the FRET signal. As a result, the substitution of Phe1014 in the BL1 to Ala (F1014A) significantly decreased the FRET signal (Fig. 6c and 6j). In addition,

F1014A mutation enhanced USP8 activity (Fig. 6d). These suggest the involvement of Phe1014 in the binding between the WW-like and USP domains.

Using structural data of the WW-like domain (Fig. 4a) and the USP domain (Fig. 6b), I performed an in silico docking simulation. I selected the most probably structural model under the condition that Phe1014 is one of the binding sites as well as that the inter-domain interaction is the most favorable (Fig. 6e). It shows a stable complex model where the WW-like domain occupies a part of the ubiquitin-binding pocket and plugs the catalytic cleft (Fig. 6f). Fig. 6g shows an enlarged view of contact sites. Tyr668 on the β-sheet of the WW-like domain forms hydrophobic contact with Phe1014 in the BL1. Thr673 in the third β-strand in the WW-like domain contacts with Leu1063 in the BL2. Asp660 and His670 in the loops between β-strands in the WW-like domain form salt bridges with Lys1011 and Gln867 in the palm subdomain, respectively. Probably by these contacts, BL1 and BL2 are relocated from their positions in ubiquitin-bound form.

Importantly, another feature of this model is that the fingers subdomain slightly bends to the inside of the ubiquitin-binding pocket, narrowing the entrance to the pocket (Fig. 6h). Pro661 in the loop between β-strands of the WW-like domain contacts with Pro955 at the base of the fingers subdomain, possibly contributing to the bending of the fingers. MD simulation confirmed that, although the fingers subdomain moves flexibly in the apo-form, it is fixed to this position in the WW-like domain bound form (Fig. 6i).

To validate this model, I carried out mutation analysis targeting two putative binding sites; Pro955 in the fingers subdomain and Leu1063 in the BL2. Combined substitution of Pro955 and Leu1063 to Ala (P955A: L1063A) decreased the FRIP8 FRET signal, although single amino acid substitution of each residue did not affect (Fig. 6j). Importantly, despite mutations in the ubiquitin-binding pocket, P955A: L1063A mutation enhanced USP8 activity (Fig. 6k). Taken together with effects of F1014A (Fig. 6c and 6d), these results clearly indicate the binding-inhibition relationship. It is noteworthy that Pro955 and Leu1063 as well as Phe1014 are highly conserved among vertebrate species (Fig. 6l).

14-3-3 proteins suppress USP8 activity by enhancing the interaction between the WW-like and USP domains

14-3-3 proteins bind to USP8 in a phosphorylation-dependent manner, then suppressing USP8 activity (Mizuno et al., 2007). Our previous laboratory member Kubo estimated

that ~60% of cellular endogenous USP8 is phosphorylated at the 14-3-3-binding motif (Kubo., 2018, Master thesis).

R18 is a peptide that inhibits 14-3-3 protein interaction with its ligands (Petosa et al., 1998). R18 treatment induced the dissociation of 14-3-3 proteins from USP8 (Fig. 7a) and enhanced USP8 activity (Fig. 7b and 7c). FRIP8 harbors the 14-3-3-binding motif between the WW-like and USP domains (Fig. 5d). Importantly, R18 treatment induced the dissociation of 14-3-3 proteins from FRIP8 (Fig. 7d), and decreased the FRET signal (Fig. 7e). These results indicate that 14-3-3 proteins enhance the interaction of the WW-like and USP domains.

Cushing's disease-associated mutations in the 14-3-3-binding motif relieve the autoinhibition

Deletion of Ser718 (ΔS718) is a representative USP8 mutation in Cushing's disease, causing the dissociation from 14-3-3 proteins (Perez-Rivas et al., 2015; Reincke et al., 2015). I confirmed that this mutation enhances USP8 activity (Fig. 8a). Importantly, I found that this mutation also induces the dissociation of 14-3-3 proteins from FRIP8 (Fig. 8b) and decreased the FRET signal (Fig. 8c). These results indicate that ΔS718 mutation enhances USP8 activity, partly through suppressing the interaction of the WW-like and USP domains.

I examined the effects of deletion of the WW-like domain and/or Ser718 on USP8 activity. Deletion of the WW-like domain enhanced USP8 activity more strongly than Ser718 deletion (Fig. 8a). It is consistent with the result that Ser718 deletion significantly but incompletely inhibited the interaction of the WW-like domain and USP domains (Fig. 8c).

A Cushing's disease-associated mutation in the WW-like domain relieves the autoinhibition

Recently, Treppiedi and his colleagues reported a new site of Cushing's disease-associated mutation apart from the 14-3-3-binding motif. The mutation they identified is a substitution of Gly664 to Arg (G664R) (Treppiedi et al., 2021), which locates at a first hairpin-like loop between β1 and β2 strands in the WW-like domain (Fig. 9a). I hypothesized that the G664R mutation might inhibit the interaction between the WW-like and USP domains and increase the availability of the USP domain. I measured the

availability using ubiquitin-viny sulfone (Ub-VS) labeling. Like Ub-VME, Ub-VS can be irreversibly conjugated to the catalytic core of USP domain (Borodovsky et al., 2001). As a result, the G664R mutation increased the availability (Fig. 9b).

I then prepared $USP8^{WT}$ and $USP8^{G664R}$ purified from HEK293 cells and measured their activities, showing that G664R mutation enhances the activity (Fig. 9c). I also prepared several USP8 deletion constructs purified from *E. coli*; $USP8^{645\text{-}1110}$ (including the WW-like and USP domain), $USP8^{645\text{-}1110}$ with the G664R mutation, and $USP8^{756\text{-}1110}$ (including only USP domain). The activity measurement showed that the G664R mutation and the lack of the WW-like domain similarly enhanced the activity (Fig. 9d), suggesting that the WW-like domain loses its function by the G664R mutation.

Next, I examined the effect of G664R mutation on the interaction between the WW-like and USP domains using FRIP8. As a result, the G664R mutation decreased the FRET signal (Fig. 9e). The complex model of the WW-like and USP domains indicates that Gly664 is at the contact site (Fig. 8f). The G664R mutation likely impairs complex formation due to steric hindrance. Taking all data together, I conclude that the G664R mutation enhances USP8 activity by inhibiting the interaction of the WW-like and USP domains.

Cushing's disease-associated mutations of USP8 affect its localization

The G664R mutation partially decreased the interaction of USP8 with 14-3-3 without affecting phosphorylation levels of the 14-3-3-binding motif (Fig. 9g). This data indicates that the functional WW-like is required for the maximum 14-3-3-binding to USP8.

Our previous member Sawada demonstrated that the 14-3-3-binding motif of USP8 can serve as a nuclear localization signal in the absence of 14-3-3, and a part of $USP8^{\Delta S718}$ localizes at the nucleus (Sawada, 2019, Master thesis). I found that $USP8^{G664R}$ localizes at the nucleus but less than $USP8^{\Delta S718}$ (Fig. 9h). Taken together, these data suggest that the G664R mutation weakly induces nuclear localization of USP8 because it partially dissociates from 14-3-3.

2.4 Discussion

In this study, I found that USP8 WW-like domain functions as a novel autoinhibitory region, by binding to the ubiquitin-binding pocket of the catalytic domain (Fig. 9i). I also found that 14-3-3 proteins bind to USP8 thereby enhancing the autoinhibitory interaction.

In cells, USP8 activity seems to be tuned by the association and dissociation of 14-3-3 proteins. In Cushing's disease, this regulation is impaired by disease-associated mutations at either the 14-3-3-binding motif or the WW-like domain. In addition, mutations of either site partially recruit USP8 into the nucleus.

The unique regulation of USP8 via the WW-like domain

In most WW domains, a few aromatic or hydrophobic side chains on its intrinsic β-sheet contact with short hydrophobic consensuses (e.g. Pro/Leu-Pro-X-Tyr) in ligand proteins (Lin et al., 2020; Salah et al., 2012). In contrast, my docking simulation highlights a distinct feature of USP8 WW-like domain; several amino acids on the β-sheet and at the peripheral loops contact with the large surface made from different subdomains of the USP domain. It is similar to the case of ubiquitin, where ubiquitin binds to USP domains through a large contact area (Ernst et al., 2013). Through this large contact, the WW-like domain appears to plug the catalytic cleft of the USP domain. In addition, probably by contacting with Pro955 in the finger subdomain, the WW-like domain changes the fingers subdomain position, thereby narrowing the entrance to the pocket. To my knowledge, USP8 is the only USP family protein with a WW-like domain, suggesting that regulation via the WW-like domain is unique to USP8.

Several USPs are reported to be regulated by the intrinsic regions that physically interact with their catalytic domains, especially their catalytic clefts. USP25 is a such DUB with its well-defined crystal structure (Gersch et al., 2019; Sauer et al., 2019). In USP25, the autoinhibitory region occupies a space between the α5 helix and the BL2. Interestingly, the autoinhibitory regions of USP8 and USP25 similarly plug an entrance to the catalytic cleft where the ubiquitin C-terminal tail should be embedded. In cases of inhibition of USPs by compounds, the similar space in USP7 and USP14 is occupied by small molecule inhibitors FT671 and IU1, respectively (Turnbull et al., 2017; Wang et al., 2018). This space may be utilized for the effective inhibition of many USPs by intrinsic regulatory motifs and chemical inhibitors.

Coordinated regulation of USP8 activity by the WW domain and 14-3-3 proteins

This study revealed that 14-3-3 proteins enhance autoinhibition by tightening the interaction between the WW-like and USP domains, thus suppressing USP8 activity. Since the 14-3-3-binding motif is located at an unstructured region between the WW-like

domain and the USP domain, it is perhaps possible that the binding might shorten the distance between these domains thereby enhancing their complex formation. Moreover, my data indicate that the functional WW-like is required for the maximum 14-3-3 binding. These findings suggest a positive feedback mechanism; 14-3-3 changes USP8 into a closed conformation by enhancing autoinhibition, and this conformation further promotes 14-3-3 binding. Further study is needed to elucidate the underlying mechanism.

New Cushing's disease-associated mutation in the WW-like domain

During my study, Treppiedi et al. reported a new Cushing's disease-associated mutation, G664R. Here, I mapped the mutated site at the WW-like domain and demonstrated that this mutation relieves the autoinhibition of USP8, a similar mechanism by which mutations of the 14-3-3-binding motif increase USP8 activity. These findings strongly support my model that relieving the autoinhibition of USP8 is underlying the pathogenic mechanism of Cushing's disease.

Accumulating genomic analyses have revealed that ~50% of Cushing's disease patients have somatic mutations of USP8, almost all of which occur at the 14-3-3-binding motif. In contrast, only one patient with mutations at the WW-like domain has been characterized (Treppiedi et al., 2021). Such mutations might rarely lead to the disease onset because mutated corticotrophs often undergo cell death due to too high USP8 activity (Fig. 8a and 9d). Large-scale genomic analysis of the entire USP8 gene region is needed.

Pathogenic mechanisms downstream of dysregulated USP8

The pathogenic mechanisms of Cushing's disease still remain unclear. Cushing's disease-associated mutations seem to induce USP8 mislocalization from the cytosol to the nucleus, raising the possibility that nuclear USP8 plays a pathogenic role. As I described above, hypersecretion of ACTH is a hallmark of Cushing's disease. Our previous laboratory member Inoko focused on the transcriptional factors promoting ACTH precursor gene expression. He found that the disease-associated USP8 mutant deubiquitinates and stabilizes a transcriptional factor Nur77 (Inoko., 2018, Master thesis). Therefore, the nuclear USP8-Nur77 pathway may be involved in the pathogenesis. Moreover, it is also important to screen USP8 substrate proteins with an unbiased approach. Our group

recently generated mice with a Cushing's disease-associated USP8 mutation by genome-editing technology and will characterize the detailed mechanisms using this model.

3. Chapter 2　Molecular basis of STAMBPL1 autoinhibition by its MIT domain and the role in apoptosis.

3.1 Introduction

STAMBP and STAMBPL1, also known as AMSH and AMSH-LP, are members of the JAMM family. Like USP8, STAMBPs localize at the endosomes (McCullough et al., 2004; Nakamura et al., 2006). STAMBPs specifically hydrolyze the Lys63-linked ubiquitin chain (McCullough et al., 2004; Sato et al., 2008), whereas USP8 can remove all types of chains from substrates.

STAMBP regulates ubiquitinated-cargo sorting system on the endosomes. STAMBP deubiquitinates EGFR and prevents its lysosomal degradation (McCullough et al., 2004). Under a specific experimental condition, STAMBP is also proposed to promote the movement of growth factor receptors to the late endosome with multiple internal vesicles (multivesicular body, MVB) (Berlin et al., 2010). Although the detailed mechanism of the latter is unclear, it is reminiscent of yeast endosomal DUB Doa4, which maintains the MVB pathway homeostasis by deubiquitinating cargos before they enter into invaginating vesicles and probably ensuring ubiquitin pool (Losko et al., 2001).

The endosomal function of STAMBPL1 has yet to be analyzed. Instead, recent studies suggest the oncogenic roles of STAMBPL1. STAMBPL1 is highly expressed in multiple cancer types. STAMBPL1 deubiquitinates and stabilizes inhibitor of apoptosis proteins (IAPs). Depletion of STAMBPL1 induces apoptosis through lysosomal degradation of X-linked IAP (XIAP) in prostate cancer (Chen et al., 2019). STAMBPL1 deubiquitinates survivin, a member of IAPs, and thus augments cell survival (Chaithongyot et al., 2022). In addition, STAMBPL1 potentiates transforming growth factor-beta (TGF-β) signaling (Ibarrola et al., 2004) and stabilizes human T-cell leukemia virus type 1 (HTLV-1) Tax oncoprotein (Lavorgna et al., 2012). STAMBPL1 is also involved in the mTOR pathway and contributes to tumorigenesis in colorectal cancer (Wang et al., 2022).

STAMBPs comprises an N-terminal MIT domain and C-terminal JAMM domain. The linker region has a clathrin-binding motif responsible for endosome localization (Nakamura et al., 2006). The MIT domain also interacts with charged multi-vesicular body proteins (CHMPs), components of endosomal sorting complexes required for transport (ESCRT)-III (Nakamura et al., 2006). The metalloprotease JAMM domain has

a core structure, including a catalytic site coordinating a zinc ion (Mevissen et al., 2017). The JAMM domain also has two insertion sequences (Ins-1 and Ins-2), which form two ubiquitin-binding sites called S1 and S1' sites for distal and proximal ubiquitin, respectively, together with the JAMM core (Sato et al., 2008). When these sites capture the Lys63-linked ubiquitin chain, the isopeptide-bond of the C-terminal tail of the distal ubiquitin is embedded near the zinc ion in the core, and then nucleophilic-attacked and hydrolyzed by a water molecule. STAMBPL1 can hydrolyze the polyubiquitin chain more efficiently than STAMBP due to a more stable complex formation between the S1 site and ubiquitin (Davies et al., 2011).

My USP8 study inspired me to search for autoinhibitory interactions between the catalytic and other domains of DUBs. By surveying AlphaFoldII-based predicted structures of all human DUBs, I discovered the MIT domain of STAMBPs as a putative autoinhibitory domain. I also found that STAMBPL1 harbors a putative caspase cleavage site in a middle region between its MIT and JAMM domains, implying cleavage-dependent regulation and its involvement in apoptosis. In this chapter, I aimed to characterize the autoinhibition of STAMBPs by the MIT domain. I also investigated the cleavage of STAMBPL1 and functionally analyzed the catalytic fragment in apoptosis.

3.2 Materials and Methods

cDNA preparation and plasmid construction

Human STAMBPL1 cDNA was amplified by PCR from U2OS cells cDNA library. Human STAMBP cDNA was prepared as described elsewhere (Mukai et al., 2008).

For the construction of expression plasmids, these cDNAs were subcloned into the following vectors; pGEX-6P1 (GE Healthcare) for the bacterial expression of N-terminal GST-tagged STAMBPL1 (full-length or aa. 197-436) and GST-tagged STAMBP (full-length or aa. 186-424); pCMV-FLAG (gift from Dr. Iwaki, Osaka University, Osaka, Japan) for the expression of C-terminal FLAG-tagged STAMBPL1 constructs; pmyc-CMV5 (gift from Dr. Nakae, Keio University, Tokyo, Japan) that I had generated by inserting FLAG peptide sequence into BamHI site for the expression of N-terminal myc- and C-terminal FLAG-tagged STAMBPL1; pEGFP-N1 (Clontech) for the expression of C-terminal GFP-tagged STAMBPL1 constructs. Site-specific mutagenesis was performed by PCR using Prime STAR mutagenesis basal kit (Takara).

Protein preparation

GST-tagged STAMBPL1 and STAMBP constructs were produced in E.coli Rosetta (DE3) pLysS cells. Protein expression was induced by the stimulation of cells with 0.5 mM IPTG, followed by overnight culture at 20 ˚C. Cells were then lysed in ice-cold lysis buffer (50 mM Tris-HCl pH 7.4, 150 mM NaCl, 50 mM NaF, 1 % Triton-X-100, 1 mM DTT) supplemented with protein inhibitors (1 μg/ml aprotinin, 1 μg/ml leupeptin and 1 μg/ml pepstatin A). After centrifugation, the supernatants were mixed with Glutathione Sepharose 4B (GE Healthcare). After 1 h incubation at 4 ˚C, beads were washed two times with lysis buffer and three times with Tris buffered saline (TBS) (20 mM Tris-HCl pH 7.4, and 150 mM NaCl), and then incubated in ice-cold elution buffer A (50 mM Tris-HCl pH 8.0 and 10 mM reduced glutathione (Wako)) at 4 ˚C for 60 min. The purity and concentration of eluates were validated by SDS-PAGE and CBB staining using Quick CBB (Wako).

Quantitative DUB assay

2 μM GST-tagged STAMBPL1 or STAMBP constructs purified from bacteria were mixed with 10 mM DTT in TBS and incubated at 37 ˚C for 10 min. Subsequently, samples were mixed with 1 μM ubiquitin-MCA (Peptide Institute) in 384 well FLUOTRAC 200 plate (Greiner). Plates were set on Varioskan LUX (Thermo Scientific), and incubated at 37 ˚C. During the incubation, fluorescence intensity of AMC released from ubiquitin was measured at 1 min intervals using 345 nm and 445 nm as excitation wavelength and emission wavelength, respectively. The fluorescence intensity of the sample without enzymes was measured as background and subtracted from each value.

***In silico* structural modeling by AlphaFold2**

Predicted human STAMBPL1 and STAMBP structures were first referred in the AlphaFold Protein Structure Database (https://alphafold.ebi.ac.uk/) and also validated using ColabFold in Google Colab called AlphaFold2 using MMseqs2. The predicted models and PAE scores reported in the AlphaFold Protein Structure Database are shown.

Caspase-cleavage site prediction

A putative caspase-cleavage site in STAMBPL1 was predicted using the Site Prediction (https://www.dmbr.ugent.be/prx/bioit2-public/SitePrediction/). Sequence similarity was

analyzed by the ClustalW program (https://clustalw.ddbj.nig.ac.jp/). Vertebrate STAMBPL1 sequences were obtained from the Uniprot Database (https://www.uniprot.org/).

Cell culture and plasmid transfection

HeLa cells were grown in Dulbecco's modified Eagle's medium (DMEM) (Nacalai Tesque) supplemented with 10 % fetal bovine serum (FBS) at 37 °C and 5 % CO_2. To induce apoptosis using tumor necrosis factor-alpha (TNF-α) with cycloheximide, HeLa cells were incubated with 10 ng/ml human TNF-α (Peprotech) and cycloheximide (Nacalai Tesque) at 37 ℃ for 6 hours or the indicated time points. To induce apoptosis using ultraviolet radiation (UV), HeLa cells were replaced into PBS, then radiated UV with 400×10^2 μJ/cm^2 intensity, again incubated in fresh DMEM at 37 ℃ for 6 hours. To inhibit caspases, HeLa cells were incubated with 10-100 μM Z-VAD-FMK (GlpBio) for pan-caspases or 10-100 μM Z-DEVD-FMK (MedChemExpress) for caspase-3 at 37 ℃ for 6 hours or the indicated time points.

Plasmids transfection was carried out using polyethyleneimine (Polyscience) according to the standard protocol. Cells were subjected to analysis 15-48 h after transfection.

Cell lysis, immunoprecipitation and immunoblotting

Cells and the cultured medium containing floating cells were centrifuged and collected. After washing with PBS, the supernatants were lysed with SDS-PAGE sample buffer (62.5 mM Tris-HCl pH 6.8, 2 % SDS, 5 % 2-mercapto ethanol, 10 % glycerol, and 0.1 mg/ml bromo phenol blue), sonicated and incubated at 98 ℃ for 5 min.

Immunoblotting were performed using standard procedures. Primary antibodies for immunoblotting were as follows: anti-STAMBPL1 antibody (clone C-11, Santa Cruz Biotechnology), anti-FLAG antibody (clone 1E6, Wako), anti-Myc antibody (clone 9E10, Wako), anti-α-tubulin antibody (clone 10G10, Wako), anti-PARP-1 antibody (clone F-2, Santa Cruz Biotechnology), anti-caspase-3 antibody (clone 31A1067, Santa Cruz Biotechnology). Secondary antibodies were peroxidase-conjugated anti-mouse IgG antibody (GE Healthcare). Blots were detected using ECL Prime Western Blotting Detection Reagents (GE Healthcare) and ImageQuant LAS 4000mini (GE Healthcare).

Live-cell imaging

HeLa cells were grown on glass-bottomed dishes and transfected GFP-tagged STAMBPL1 constructs. After 15 h transfection, fluorescence images of GFP sequentially acquired using THUNDER Imager (Leica) with a FITC-channel. The images were optimized by THUNDER Computational Clearing algorithm.

Living cell counting assay

Counting living cells was preformed using Cell Counting Kit-8 (DOJINDO) according to the manufacture's protocol. After HeLa cells were transfected STAMBPL1 constructs, the cultured medium was stained with WST-8 formazan. The absorbance was measured using Varioskan LUX (Thermo Scientific) and analyzed using Prism 9 (GraphPad Software).

Dead cell counting assay

After HeLa cells were transfected STAMBPL1 constructs, the cells were stained with 1 mM SYTOX Green (Invitrogen) at 37 ℃ for 2 h. The fluorescence was measured using Varioskan LUX (Thermo Scientific) using an excitation filter of 485 nm and an emission filter of 520 nm, and analyzed using Prism 9 (GraphPad Software). The percentage of cell death was calculated as the intensity of (induced fluorescence-background fluorescence)/(maximal fluorescence-background fluorescence)x100. The maximal fluorescence is obtained by full permeabilization of the cells by using Triton X-100 at a final concentration of 0.1%.

FACS analysis

Determining type of cell death by Ct-STAMBPL1 overexpression in HeLa cells was preformed using Annexin V-FITC/propidium iodide (PI) apoptosis detection kit (Nacalai Tesque) according to the manufacture's protocol. After HeLa cells were transfected STAMBPL1 constructs, the cells were collected, washed with PBS and then stained with Annexin V-FITC and PI. The fluorescence was measured and analyzed using Cell Sorter SH800S (SONY).

Statistical analysis

The results shown are the mean±s.d. Data were analyzed by one-way factorial analysis of variance followed by Tukey–Kramer post-hoc multiple comparison test. The significance level of $P < 0.05$ shows statistically significant.

3.3 Results

The MIT domain of STAMBPs is autoinhibitory

First, I examined whether the MIT domain of STAMBPL1 is autoinhibitory. I measured the enzyme activity of GST-tagged STAMBPL1 ($STAMBPL1^{WT}$) and the truncated mutant lacking the MIT domain ($STAMBPL1^{\Delta MIT}$). As expected, $STAMBPL1^{\Delta MIT}$ showed higher activity than $STAMBPL1^{WT}$ (Fig. 10a).

The full-length STAMBPL1 structure predicted by AlphaFold2 (Jumper et al., 2021) shows a closed conformation in which the MIT domain, like a mallet (kine), interacts with the JAMM domain, like a rice mortar (usu), with low PAE values (Fig. 10b and 10c). This conformation is evolutionarily conserved among the predicted structures of all STAMBPL1 orthologs, including yeast SST2, referred in the AlphaFold2 database (Tunyasuvunakool et al., 2021). The full-length STAMBPL1 structure was superimposed with a crystal structure of the STAMBPL1 JAMM domain in complex with Lys63-linked ubiquitin dimer (Sato et al., 2008). I found that the MIT domain blocks the distal ubiquitin-binding site (S1 site) (Fig. 10b). Specifically, Arg49, Arg53, Glu57, Arg60, Tyr65, and Glu68 in an α-helix in the MIT domain interact with residues forming the S1 site via hydrogen bonds (Fig. 10d). The substitution of contact residues in the MIT domain to Ala increased STAMBPL1 activity (Fig. 9e), confirming the structure-inhibition relationship.

Similarly, the predicted structure of full-length STAMBP also showed a closed conformation (Fig. 10f). The STAMBP truncated mutant lacking the MIT domain ($STAMBP^{\Delta MIT}$) showed higher activity than the full-length (Fig. 10g). Taking together, I concluded that STAMBPs have an autoinhibitory MIT domain.

STAMBPL1 MIT domain is cleaved off by caspase-3 during apoptosis

I found that STAMBPL1 has a putative caspase cleavage site (SEQIDG; aa. 204-210) using Site Prediction (Verspurten et al., 2009). This site is mapped in the linker region between the MIT and JAMM domains and is highly conserved among vertebrates (Fig. 11a). STAMBP has no homologous sequence.

Next, I tested whether STAMBPL1 is a target for caspases. HeLa cells were stimulated with tumor necrosis factor-alpha (TNF-α) and cycloheximide (CHX) to activate the extrinsic apoptosis pathway. Immunoblot analysis using an antibody against the C-terminal region of STAMBPL1 (aa. 171-280) revealed that ~28 kDa fragment of endogenous STAMBPL1 was generated upon the stimulation and was abolished by the additional treatment with a pan-caspase inhibitor Z-VAD-FMK (Fig. 11b). I named this C-terminal fragment Ct-STAMBPL1.

The exogenously expressed STAMBPL1 was also cleaved upon the stimulation with TNF-α and CHX in a caspase-dependent manner (Fig. 11c). A small amount of Ct-STAMBPL1 was detected under basal conditions, possibly due to partial activation of the apoptosis pathway resulting from the stress of gene overexpression. Ultraviolet radiation, which activates the intrinsic apoptosis pathway, also generated Ct-STAMBPL1 in a caspase-dependent manner (Fig. 11c). The substitution of Asp207, putative cleavage site, by Ala abolished STAMBPL1 cleavage (Fig. 11d). Caspase-3 is an executioner caspase involved in both extrinsic and intrinsic apoptosis pathways (Elmore., 2007). A caspase-3 specific inhibitor Z-DEVD-FMK inhibited STAMBPL1 cleavage (Fig. 11e). Together, these results indicate that STAMBPL1 is cleaved by caspase-3 at the Asp207 during apoptosis.

Ct-STAMBPL1 is enriched in the plasma membrane, possibly via N-myristoylation

Cellular proteins can be modified with N-myristoylation if the N-terminal sequence matches the lenient myristoylation motif (Gly-X-X-X-Ser/Thr) (Johnson et al., 1994; Udenwobele et al., 2017). Ct-STAMBPL1 has this motif, and the corresponding sequences are conserved among vertebrates (Fig. 11f). A previous report made a list of N-myristoylated proteins in apoptotic cells using large-scale proteomics analysis (Thinon et al., 2014), and I found out Ct-STAMBPL1 in the list.

Since N-myristoylation functions as a plasma membrane target signal, I checked Ct-STAMBPL1 localization. Full-length STAMBPL1 was observed in the nucleus and cytosol and at the cytosolic spots, possibly endosomes, as previous report (McCullough et al., 2004; Nakamura et al., 2006) (Fig. 11g, left). Ct-STAMBPL1 was enriched in the plasma membrane (Fig. 11g, middle). The substitution of Gly208 by Ala, which would inhibit N-myristoylation, decreased the plasma membrane localization (Fig. 11g, right).

These results suggest that Ct-STAMBPL1 preferentially localizes at the plasma membrane, possibly via N-myristoylation.

Ct-STAMBPL1 has the ability to induce apoptosis by itself

In the experiment shown in Fig. 11g, most cells transfected with Ct-STAMBPL1 eventually underwent apoptosis-like morphological changes (data not shown). Therefore, I investigated the effects of Ct-STAMBPL1 on cell survival and death. To clarify the requirement of DUB activity, I prepared a construct of catalytically inactive Ct-STAMBPL1 in which Asp360 in the catalytic site (Sato et al., 2008) is substituted by Ala (Ct-STAMBPL1^{D360A}). Under cell culture conditions without apoptotic inducers, living cell and dead cell numbers were decreased and increased, respectively, by overexpression of Ct-STAMBPL1, while they were little changed by full-length STAMBPL1 and Ct-STAMBPL1^{D360A} (Fig. 12a and 12b). The increase in cell survival by Ct-STAMBPL1 was comparable to that by TNF-α and CHX and was suppressed by Z-VAD-FMK (Fig. 12a).

Overexpression of Ct-STAMBPL1 induced the cleavage of executioner caspase-3 (i.e., activation) (Fig. 12c, middle). It also yielded the cleavage of poly (ADP-ribose) polymerase (PARP), a caspase-3 target (Fig. 12c, lower). These changes did not occur by STAMBPL1^{D360A} (Fig. 12c). Finally, I performed FACS analysis using Annexin V-propidium iodide (PI) staining. Overexpression of Ct-STAMBPL1 moderately increased early apoptotic cells (Annexin V-FITC^{+}/PI^{-} cells) and intensely increased late apoptotic or necrotic cells (Annexin V-FITC^{+}/PI^{+} cells) (Fig. 12d). These data suggest that Ct-STAMBPL1 activates the caspase pathway depending on its catalytic activity, thereby promoting apoptosis.

3.4 Discussion

In this chapter, I showed that STAMBPs have an autoinhibitory MIT domain. I also identified STAMBPL1 as a caspase-3 substrate during apoptosis. Caspase-3 cleaves STAMBPL1 at the linker region between the MIT and JAMM domains, generating Ct-STAMBPL1 that is relieved from autoinhibition. Ct-STAMBPL1 preferentially localizes at the plasma membrane, possibly via N-myristoylation. Ct-STAMBPL1 has the ability to promote apoptosis through its deubiquitinase activity (Fig. 12e).

The functional regulation of full-length STAMBPs by the MIT domain interacting with the JAMM domain

I showed that the MIT domain inhibits STAMBPs' enzyme activity via direct binding to the S1 site in the JAMM domain. I evaluated their activity using ubiquitin-AMC as a substrate, and the effects of the interaction between the MIT and JAMM domains on their ubiquitin chain-type specificity remain unclear. The specificity of STAMBPs for the Lys63 chain is defined by the steric configuration of the S1 and S1' sites (Sato et al., 2008). This configuration in the predicted structure of full-length STAMBPL1 was similar to that in the complex formed by the STAMBPL1 JAMM domain and ubiquitin dimer (Fig. 10b). Therefore, the interaction of the MIT domain may little affect their chain specificity.

CHMPs interact with the MIT domain of STAMBP and may play an essential role in the STAMBP-mediated degradation of endosomal proteins (Ma et al., 2007). Although the CHMP-binding site in the MIT domain of STAMBP (Solomons et al., 2011) is not overlapped with the contact site to the JAMM domain, it should be analyzed if the JAMM domain affects the binding of the MIT domain to CHMPs and vice versa. The physiological significance of autoinhibition of full-length STAMBPs will be discussed in the General Discussion.

Caspase-dependent regulation of STAMBPL1

To my knowledge, this is the first report that DUB activity is regulated by caspase-3-dependent cleavage. I showed that the cleavage product Ct-STAMBPL1, in turn, increases caspase-3 activation, indicating positive feedback regulation. I also determined the caspase cleavage site of STAMBPL1 (aa. 204-210). Noteworthily, it is near the clathrin-binding site (aa. 154-181) (Nakamura et al., 2006), suggesting that clathrin may inhibit the cleavage reaction of STAMBPL1.

Furthermore, the caspase-dependent cleavage of STAMBPL1 is coupled with Ct-STAMBPL1 transport to the plasma membrane. Because the most likely underlying mechanism of the transport is N-myristoylation, I will test the effect of N-myristoyltransferase inhibitor on Ct-STAMBPL1 localization and the pro-apoptotic function.

Anti- and pro-apoptotic functions of STAMBPL1 and their switching by caspase-dependent cleavage

Previous reports suggested that STAMBPL1 functions as an anti-apoptotic activity in several cancer cells through its deubiquitinase activity. Some IAPs are possibly modified with Lys48/Lys63 branched ubiquitin chain (Akizuki et al., 2022), and STAMBPL1 stabilizes IAPs (Chen et al., 2019; Chaithongyot et al., 2022), probably via deubiquitinating the Lys63-linkage. STAMBPL1 also deubiquitinates Sestrin2 and relieves ubiquitinated Sestrin2-dependent inhibition of the mTOR signal (Wang et al., 2022). In contrast, here I showed that Ct-STAMBPL1 exhibit pro-apoptotic activity. Therefore, STAMBPL1 has dual functions in regulating apoptosis. Switching between these functions is mediated by activation of the caspase pathway.

Further studies using more physiological conditions (e.g., cells with STAMBPL1 knockdown and re-expression of non-cleaved STAMBPL1^{D207A}) are needed to clarify the significance of endogenous Ct-STAMBPL1 in apoptosis. Moreover, I will identify plasma membrane proteins that Ct-STAMBPL1 deubiquitinates to understand the underlying mechanism of Ct-STAMBPL1 pro-apoptotic function.

The relief of STAMBP autoinhibition by MIC-CAP syndrome-associated mutations

This study also shows that the autoinhibitory MIT domain regulates not only STAMBPL1 but also STAMBP. MIC-CAP syndrome is characterized by an abnormally small head size (MICrocephaly) and abnormalities of small CAPillary in the skin. As I described in the General Introduction, it is an autosomal recessive disorder caused by biallelic loss-of-function mutations of STAMBP (McDonell et al., 2013). These mutations are frequently found in the MIT and JAMM domains. The representative mutations in the MIT domain are substitutions of Arg38 by Cys and Glu42 by Gly (McDonell et al., 2013). Interestingly, the predicted structure suggests that these residues are involved in the contact between the MIT and JAMM domains, implying the relief of autoinhibition. In patients, these mutations significantly destabilize the STAMBP protein (McDonell et al., 2013). Further studies are needed to elucidate the relationship between the relief of autoinhibition and destabilization.

4. General discussion

4.1 Cis-regulatory mechanisms of DUBs

In general, the catalytic activity of many proteases is tightly regulated so that they hydrolyze only specific substrate proteins. The cis-regulation mechanism of some proteases, including caspases, lysosomal proteases, and digestive enzymes like trypsin, have been well-characterized. In contrast, the cis-regulation of DUBs has only recently begun to be analyzed. USP4 and USP7 harbor intrinsic domains required for their full catalytic activity. These domains interact with USP domains, activating them through allosteric mechanisms (Clerici et al., 2014; Faesen et al., 2011; Kim et al., 2019). On the other hand, other researchers and I have identified the intrinsic inhibitory sequences/domains of DUBs. Here, I compared their inhibition mechanisms.

Short loops intrinsic to the catalytic domains, including the blocking loops in some USPs and the crossover loops in UCHs (UCHL5 and BAP1), inhibit the accession of ubiquitin to the enzyme active sites. The binding of ubiquitin to the ubiquitin-binding pocket of USP domains causes the rearrangement of the blocking loops and enzyme activation (i.e., substrate-induced conformational change) (Avvakumov et al., 2006). UCHL5 is a proteasome-associated DUB, and BAP1 is a catalytic subunit of the Polycomb repressive deubiquitinase complex (PR-DUB) that regulates Polycomb-mediated gene repression. When a proteasomal subunit RPN13 binds to UCHL5 and a PR-DUB subunit ASHL1 binds to BAP1, the crossover loops are rearranged, resulting in enzyme activation (Sahtoe et al., 2015; Sahtoe et al., 2016). Thus, these mechanisms enable UCH activation only in the macromolecular protein complexes.

Long inserted sequences to the surface of the USP domains can regulate their enzyme activity. USP1 is involved in DNA repair pathway, and its activity is enhanced upon binding DNA. Approximately 200 amino acid insertion (called insert L1) of USP1 mediates USP1-DNA interaction (Lim et al., 2018), although the structural basis remains unclear. USP25 is a multifunctional DUB and have a ~180 amino acid insertion (called AIM) in the USP domain. USP25 can form auto-inhibited tetramer in which the AIM interacts with the ubiquitin-binding pocket (Gersch et al., 2019; Sauer et al., 2019), although its physiological significance has not been defined.

USP30 functions on the mitochondrial outer membrane. A peptide derived from the USP30 trans-membrane (TM) region can inhibit its enzyme activity (Qin et al., 2022).

The authors suggested an attractive on-site activation mechanism; cytosolic USP30 is autoinhibited by the TM region, and mitochondrial USP30 is activated because the TM region integrates into the membrane.

As described above, autoinhibitory sequences of some DUBs directly interact with the ubiquitin-binding sites of the enzyme domain, similar to USP8 and STAMBPs. In some cases, the interaction with specific proteins or lipids relieves autoinhibition, allowing conditional activation of DUBs. Until now, it is unknown whether some factors may activate USP8 or STAMBPs in a similar mechanism. However, the WW domain is generally known to interact with proline-rich proteins (Salah et al., 2012), and the MIT domain of STAMBPs can interact with CHMPs (Kyuuyama et al., 2007; Tsang et al., 2006). Thus, these binding proteins might activate USP8 and STAMBPs. In the next section, I will discuss the physiological significance of these putative mechanisms. In the case of USP8, 14-3-3-binding enhances the autoinhibitory interaction between the WW-like and USP domains. It is the first case where a trans-factor enhances the autoinhibition of DUB, and its structural basis should be determined.

4.2 Roles of autoinhibition mechanism of DUBs in acquiring their substrate specificity

Many PTMs, such as phosphorylation, occur on specific sequence motifs. In contrast, no motifs have been identified for ubiquitination. Therefore, many DUB must acquire substrate specificity by recognizing substrate moieties other than ubiquitination sites or localizing at specific compartments. In general, the autoinhibition sequence is useful for keeping enzyme activity off under basal conditions and rapid on-off switching. Functional linkage of the substrate recognition and/or localization domains with autoinhibition sequences appears to be the best strategy for acquiring substrate specificity of DUBs.

Ubiquitination targets many plasma membrane proteins, such as growth factor receptors, to the endocytosis pathway (Fig. 13a). Deubiquitination of these proteins at the early and late endosomes is involved in their recycling to the plasma membrane and lysosomal degradation, respectively (Clague et al., 2006; Williams et al., 2007). USP8, STAMBP, and STAMBPL1 are the responsible DUBs for these regulations (Clague et al., 2006; Williams et al., 2007). HRS is a component of the ESCRT-0 complex localizing at the early endosome. Interestingly, HRS harbors a hydrophobic motif (Leu-Pro-X-Tyr) that putatively binds to the WW-like domain of USP8 (Kakihara, unpublished data).

CHMPs, components of the ESCRT-III complex localizing at the late endosome, interact with the MIT domain of STAMBPs (Kyuuyama et al., 2007; Tsang et al., 2006). I provide an attractive model that, upon binding to ESCRT proteins, USP8 and STAMBPs are relieved from autoinhibition, thereby activating in a site-specific manner (Fig. 13a).

Similarly, USP30 is proposed to be relieved from autoinhibition upon binding to the mitochondrial membrane, as described above (Qin et al., 2022). Although further study is needed, many DUBs likely have an autoinhibition mechanism involved in acquiring substrate specificity.

4.3 Relieving autoinhibition mechanism of DUBs in diseases and cell death

Given the significant functions of DUBs, it is easy to understand how loss-of-function mutations in DUBs cause various diseases. On the other hand, how do gain-of-function mutations of some DUBs cause diseases? I identified that Cushing's disease-associated USP8 mutations induce its constitutive activation (relieve of autoinhibition). Based on my idea that the autoinhibition mechanism of USP8 may be required for its site-specific activation, USP8 mutations may lead to the deubiquitination of many proteins in the cytosol. In addition, the USP8 mutations caused partial mislocalization into the nuclear, possibly resulting in the deubiquitination of nuclear proteins as well as cytosolic proteins.

Interestingly, a group of Cushing's disease patients has somatic mutations in USP48 (Chen et al., 2018), a nuclear DUB involved in the DNA repair pathway (Kee et al., 2016; Le et al., 2019). Like USP8, the mutations of USP48 also increase its enzyme activity (Chen et al., 2018). Why are the mutations of the two DUBs with quite different cellular functions related to Cushing's disease? The most attractive hypothesis is that loss of DUB substrate specificity followed by non-specific deubiquitination is the underlying mechanism of Cushing's disease. To test it, identifying substrate proteins of mutated USP8 and USP48 is essential.

Relieving autoinhibition of STAMBPL1 by cleavage is involved in apoptosis. Again, the release of autoinhibition may lower its substrate specificity. Furthermore, the cleavage of STAMBPL1 is coupled with its translocation to the plasma membrane. To understand the pro-apoptotic mechanisms, I need to explore and compare the substrates of full-length STAMBPL1 and Ct-STAMBPL1. DUBs lacking substrate specificity may be cytotoxic. The cells appear to take advantage of this dangerous molecule to induce apoptosis.

4.4 Prospects for developing tools to manipulate DUB activity

This study provides a molecular basis for developing methods to regulate DUB's activity. Inhibitors of USP8 (and USP48) are expected for the therapy of Cushing's disease. However, due to the structural similarity of active centers among USPs, it is challenging to develop isoform-specific USP inhibitors acting on the active centers. I propose molecules mimicking the autoinhibition sequence of USP8 as potential USP8 inhibitors. A similar strategy was already successful in making USP30 inhibitors (Qin et al., 2022). On the other hand, compounds interacting with the MIT domain of STAMBPL1 may inhibit its interaction with the catalytic domain, thereby activating STAMBPL1. If this compound, like Ct-STAMBPL1, can induce apoptosis, it may be used as a tool to induce apoptotic cell death of unfavorable cells, such as cancer cells.

4.5 Conclusion

In this study, I identified autoinhibitory domains of USP8 and STAMBPs and revealed their cis-regulations of enzyme activities. Under physiological situations, these autoinhibitions should be relieved only where and when their full catalytic activities are required. These regulations of USP8 and STAMBPs possibly enable proper sorting and transport of endosomal proteins. The regulation of STAMBPL1 is also necessary for STAMBPL1 to function as an anti-apoptotic factor. On the other hand, relieving these autoinhibitions is associated with the onset of Cushing’s disease and apoptotic signaling, respectively. Dysfunction of USP8 autoinhibition by the disease-associated mutations results in a constitutive relief of the autoinhibition, over-activating its enzyme activity. Caspase-dependent cleavage of STAMBPL1 relieves the autoinhibition, thus switching the STAMBPL1 role to a pro-apoptotic factor. This study sheds light on the importance of DUB activity regulation and provides molecular bases to develop new tools for manipulating DUB activity and therapeutics for DUB-associated diseases.

5. References

Adorno, M., Sikandar, S., Mitra, S.S., Kuo, A., Nicolis Di Robilant, B., Haro-Acosta, V., Ouadah, Y., Quarta, M., Rodriguez, J., Qian, D., et al. (2013). Usp16 contributes to somatic stem-cell defects in Down's syndrome. Nature 501, 380-384.

Adoro, S., Park, K.H., Bettigole, S.E., Lis, R., Shin, H.R., Seo, H., Kim, J.H., Knobeloch, K.P., Shim, J.H., and Glimcher, L.H. (2017). Post-translational control of T cell development by the ESCRT protein CHMP5. Nat Immunol 18, 780-790.

Akizuki, Y., Morita, M., Mori, Y., Kaiho-Soma, A., Dixit, S., Endo, A., Shimogawa, M., Hayashi, G., Naito, M., Okamoto, A., et al. (2022). cIAP1-based degraders induce degradation via branched ubiquitin architectures. Nat Chem Biol.

Avvakumov, G.V., Walker, J.R., Xue, S., Finerty, P.J., Jr., Mackenzie, F., Newman, E.M., and Dhe-Paganon, S. (2006). Amino-terminal dimerization, NRDP1-rhodanese interaction, and inhibited catalytic domain conformation of the ubiquitin-specific protease 8 (USP8). J Biol Chem 281, 38061-38070.

Berlin, I., Higginbotham, K.M., Dise, R.S., Sierra, M.I., and Nash, P.D. (2010). The deubiquitinating enzyme USP8 promotes trafficking and degradation of the chemokine receptor 4 at the sorting endosome. J Biol Chem 285, 37895-37908.

Berlin, I., Schwartz, H., and Nash, P.D. (2010). Regulation of epidermal growth factor receptor ubiquitination and trafficking by the USP8.STAM complex. J Biol Chem 285, 34909-34921.

Borodovsky, A., Kessler, B.M., Casagrande, R., Overkleeft, H.S., Wilkinson, K.D., and Ploegh, H.L. (2001). A novel active site-directed probe specific for deubiquitylating enzymes reveals proteasome association of USP14. EMBO J 20, 5187-5196.

Borodovsky, A., Ovaa, H., Kolli, N., Gan-Erdene, T., Wilkinson, K.D., Ploegh, H.L., and Kessler, B.M. (2002). Chemistry-based functional proteomics reveals novel members of the deubiquitinating enzyme family. Chem Biol 9, 1149-1159.

Cendrowski, J., Mamińska, A., and Miaczynska, M. (2016). Endocytic regulation of cytokine receptor signaling. Cytokine Growth Factor Rev 32, 63-73.

Centorrino, F., Ballone, A., Wolter, M., and Ottmann, C. (2018). Biophysical and structural insight into the USP8/14-3-3 interaction. FEBS Lett 592, 1211-1220.

Chaithongyot, S., and Naumann, M. (2022). Helicobacter pylori-induced reactive oxygen species direct turnover of CSN-associated STAMBPL1 and augment apoptotic cell death. Cell Mol Life Sci 79, 86.

Chen, J., Jian, X., Deng, S., Ma, Z., Shou, X., Shen, Y., Zhang, Q., Song, Z., Li, Z., Peng, H., et al. (2018). Identification of recurrent USP48 and BRAF mutations in Cushing's disease. Nat Commun 9, 3171.

Chen, X., Shi, H., Bi, X., Li, Y., and Huang, Z. (2019). Targeting the deubiquitinase STAMBPL1 triggers apoptosis in prostate cancer cells by promoting XIAP degradation. Cancer Lett 456, 49-58.

Clague, M.J., and Urbé, S. (2006). Endocytosis: the DUB version. Trends Cell Biol 16, 551-559.

Clague, M.J., Urbe, S., and Komander, D. (2019). Breaking the chains: deubiquitylating enzyme specificity begets function. Nat Rev Mol Cell Biol 20, 338-352.

Clerici, M., Luna-Vargas, M.P., Faesen, A.C., and Sixma, T.K. (2014). The DUSP-Ubl domain of USP4 enhances its catalytic efficiency by promoting ubiquitin exchange. Nat Commun 5, 5399.

Crespo-Yanez, X., Aguilar-Gurrieri, C., Jacomin, A.C., Journet, A., Mortier, M., Taillebourg, E., Soleilhac, E., Weissenhorn, W., and Fauvarque, M.O. (2018). CHMP1B is a target of USP8/UBPY regulated by ubiquitin during endocytosis. PLoS Genet 14, e1007456.

Damgaard, R.B., Walker, J.A., Marco-Casanova, P., Morgan, N.V., Titheradge, H.L., Elliott, P.R., McHale, D., Maher, E.R., McKenzie, A.N.J., and Komander, D. (2016). The Deubiquitinase OTULIN Is an Essential Negative Regulator of Inflammation and Autoimmunity. Cell 166, 1215-1230.e1220.

Dang, L.C., Melandri, F.D., and Stein, R.L. (1998). Kinetic and mechanistic studies on the hydrolysis of ubiquitin C-terminal 7-amido-4-methylcoumarin by deubiquitinating enzymes. Biochemistry 37, 1868-1879.

Davies, C.W., Paul, L.N., Kim, M.I., and Das, C. (2011). Structural and thermodynamic comparison of the catalytic domain of AMSH and AMSH-LP: nearly identical fold but different stability. J Mol Biol 413, 416-429.

Dikic, I., and Schulman, B.A. (2022). An expanded lexicon for the ubiquitin code. Nat Rev Mol Cell Biol, 1-15.

Durcan, T.M., Tang, M.Y., Perusse, J.R., Dashti, E.A., Aguileta, M.A., McLelland, G.L., Gros, P., Shaler, T.A., Faubert, D., Coulombe, B., et al. (2014). USP8 regulates mitophagy by removing K6-linked ubiquitin conjugates from parkin. EMBO J 33, 2473-2491.

Elliott, P.R., Leske, D., Wagstaff, J., Schlicher, L., Berridge, G., Maslen, S., Timmermann, F., Ma, B., Fischer, R., Freund, S.M.V., et al. (2021). Regulation of CYLD activity and specificity by phosphorylation and ubiquitin-binding CAP-Gly domains. Cell Rep 37, 109777.

Elmore, S. (2007). Apoptosis: a review of programmed cell death. Toxicol Pathol 35, 495-516.

Ernst, A., Avvakumov, G., Tong, J., Fan, Y., Zhao, Y., Alberts, P., Persaud, A., Walker, J.R., Neculai, A.M., Neculai, D., et al. (2013). A strategy for modulation of enzymes in the ubiquitin system. Science 339, 590-595.

Faesen, A.C., Dirac, A.M., Shanmugham, A., Ovaa, H., Perrakis, A., and Sixma, T.K. (2011). Mechanism of USP7/HAUSP activation by its C-terminal ubiquitin-like domain and allosteric regulation by GMP-synthetase. Mol Cell 44, 147-159.

Gersch, M., Wagstaff, J.L., Toms, A.V., Graves, B., Freund, S.M.V., and Komander, D. (2019). Distinct USP25 and USP28 Oligomerization States Regulate Deubiquitinating Activity. Mol Cell 74, 436-451 e437.

Gu, H., Shi, X., Liu, C., Wang, C., Sui, N., Zhao, Y., Gong, J., Wang, F., Zhang, H., Li, W., et al. (2019). USP8 maintains embryonic stem cell stemness via deubiquitination of EPG5. Nat Commun 10, 1465.

Harbour, J.W., Onken, M.D., Roberson, E.D., Duan, S., Cao, L., Worley, L.A., Council, M.L., Matatall, K.A., Helms, C., and Bowcock, A.M. (2010). Frequent mutation of BAP1 in metastasizing uveal melanomas. Science 330, 1410-1413.

Hu, M., Li, P., Li, M., Li, W., Yao, T., Wu, J.W., Gu, W., Cohen, R.E., and Shi, Y. (2002). Crystal structure of a UBP-family deubiquitinating enzyme in isolation and in complex with ubiquitin aldehyde. Cell 111, 1041-1054.

Hu, M., Li, P., Song, L., Jeffrey, P.D., Chenova, T.A., Wilkinson, K.D., Cohen, R.E., and Shi, Y. (2005). Structure and mechanisms of the proteasome-associated deubiquitinating enzyme USP14. EMBO J 24, 3747-3756.

Ibarrola, N., Kratchmarova, I., Nakajima, D., Schiemann, W.P., Moustakas, A., Pandey, A., and Mann, M. (2004). Cloning of a novel signaling molecule, AMSH-2, that potentiates transforming growth factor beta signaling. BMC Cell Biol 5, 2.

Kato, M., Miyazawa, K., and Kitamura, N. (2000). A deubiquitinating enzyme UBPY interacts with the Src homology 3 domain of Hrs-binding protein via a novel binding motif PX(V/I)(D/N)RXXKP. J Biol Chem 275, 37481-37487.

Kawaguchi, K., Uo, K., Tanaka, T., and Komada, M. (2017). Tandem UIMs confer Lys48 ubiquitin chain substrate preference to deubiquitinase USP25. Sci Rep 7, 45037.

Kee, Y., and Huang, T.T. (2016). Role of Deubiquitinating Enzymes in DNA Repair. Mol Cell Biol 36, 524-544.

Kim, R.Q., Geurink, P.P., Mulder, M.P.C., Fish, A., Ekkebus, R., El Oualid, F., van Dijk, W.J., van Dalen, D., Ovaa, H., van Ingen, H., and Sixma, T.K. (2019). Kinetic analysis of multistep USP7 mechanism shows critical role for target protein in activity. Nat Commun 10, 231.

Komada, M., and Kitamura, N. (1995). Growth factor-induced tyrosine phosphorylation of Hrs, a novel 115-kilodalton protein with a structurally conserved putative zinc finger domain. Mol Cell Biol 15, 6213-6221.

Komander, D., and Rape, M. (2012). The ubiquitin code. Annu Rev Biochem 81, 203-229.

Komander, D., Clague, M.J., and Urbe, S. (2009). Breaking the chains: structure and function of the deubiquitinases. Nat Rev Mol Cell Biol 10, 550-563.

Komatsu, N., Aoki, K., Yamada, M., Yukinaga, H., Fujita, Y., Kamioka, Y., and Matsuda, M. (2011). Development of an optimized backbone of FRET biosensors for kinases and GTPases. Mol Biol Cell 22, 4647-4656.

Kyuuma, M., Kikuchi, K., Kojima, K., Sugawara, Y., Sato, M., Mano, N., Goto, J., Takeshita, T., Yamamoto, A., Sugamura, K., and Tanaka, N. (2007). AMSH, an ESCRT-III associated enzyme, deubiquitinates cargo on MVB/late endosomes. Cell Struct Funct 31, 159-172.

Lavorgna, A., and Harhaj, E.W. (2012). An RNA interference screen identifies the Deubiquitinase STAMBPL1 as a critical regulator of human T-cell leukemia virus type 1 tax nuclear export and NF-κB activation. J Virol 86, 3357-3369.

Le Clorennec, C., Lazrek, Y., Dubreuil, O., Larbouret, C., Poul, M.A., Mondon, P., Melino, G., Pelegrin, A., and Chardes, T. (2016). The anti-HER3 (ErbB3) therapeutic antibody 9F7-F11 induces HER3 ubiquitination and degradation in tumors through JNK1/2- dependent ITCH/AIP4 activation. Oncotarget 7, 37013-37029.

Le, J., Perez, E., Nemzow, L., and Gong, F. (2019). Role of deubiquitinases in DNA damage response. DNA Repair (Amst) 76, 89-98.

Levkowitz, G., Waterman, H., Zamir, E., Kam, Z., Oved, S., Langdon, W.Y., Beguinot, L., Geiger, B., and Yarden, Y. (1998). c-Cbl/Sli-1 regulates endocytic sorting and ubiquitination of the epidermal growth factor receptor. Genes Dev 12, 3663-3674.

Levskaya, A., Weiner, O.D., Lim, W.A., and Voigt, C.A. (2009). Spatiotemporal control of cell signalling using a light-switchable protein interaction. Nature 461, 997-1001.

Li, H., Lim, K.S., Kim, H., Hinds, T.R., Jo, U., Mao, H., Weller, C.E., Sun, J., Chatterjee, C., D'Andrea, A.D., et al. (2016). Allosteric Activation of Ubiquitin-Specific Proteases by beta-Propeller Proteins UAF1 and WDR20. Mol Cell 63, 249-260.

Li, S., Chen, Y., Shi, Q., Yue, T., Wang, B., and Jiang, J. (2012). Hedgehog-regulated ubiquitination controls smoothened trafficking and cell surface expression in Drosophila. PLoS Biol 10, e1001239.

Lim, K.S., Li, H., Roberts, E.A., Gaudiano, E.F., Clairmont, C., Sambel, L.A., Ponnienselvan, K., Liu, J.C., Yang, C., Kozono, D., et al. (2018). USP1 Is Required for Replication Fork Protection in BRCA1-Deficient Tumors. Mol Cell 72, 925-941.e924.

Lin, Z., Xie, R., Guan, K., and Zhang, M. (2020). A WW Tandem-Mediated Dimerization Mode of SAV1 Essential for Hippo Signaling. Cell Rep 32, 108118.

Losko, S., Kopp, F., Kranz, A., and Kölling, R. (2001). Uptake of the ATP-binding cassette (ABC) transporter Ste6 into the yeast vacuole is blocked in the doa4 Mutant. Mol Biol Cell 12, 1047-1059.

Ma, G., Li, S., Han, Y., Li, S., Yue, T., Wang, B., and Jiang, J. (2016). Regulation of Smoothened Trafficking and Hedgehog Signaling by the SUMO Pathway. Dev Cell 39, 438-451.

Ma, Y.M., Boucrot, E., Villén, J., Affar, E.B., Gygi, S.P., Göttlinger, H.G., and Kirchhausen, T. (2007). Targeting of AMSH to endosomes is required for epidermal growth factor receptor degradation. J Biol Chem 282, 9805-9812.

Ma, Z.Y., Song, Z.J., Chen, J.H., Wang, Y.F., Li, S.Q., Zhou, L.F., Mao, Y., Li, Y.M., Hu, R.G., Zhang, Z.Y., et al. (2015). Recurrent gain-of-function USP8 mutations in Cushing's disease. Cell Res 25, 306-317.

McCullough, J., Clague, M.J., and Urbé, S. (2004). AMSH is an endosome-associated ubiquitin isopeptidase. J Cell Biol 166, 487-492.

McDonell, L.M., Mirzaa, G.M., Alcantara, D., Schwartzentruber, J., Carter, M.T., Lee, L.J., Clericuzio, C.L., Graham, J.M., Morris-Rosendahl, D.J., Polster, T., et al. (2013). Mutations in STAMBP, encoding a deubiquitinating enzyme, cause microcephaly-capillary malformation syndrome. Nat Genet 45, 556-562.

Mevissen, T.E.T., and Komander, D. (2017). Mechanisms of Deubiquitinase Specificity and Regulation. Annu Rev Biochem 86, 159-192.

Mizuno, E., Iura, T., Mukai, A., Yoshimori, T., Kitamura, N., and Komada, M. (2005). Regulation of epidermal growth factor receptor down-regulation by UBPY-mediated deubiquitination at endosomes. Mol Biol Cell 16, 5163-5174.

Mizuno, E., Kawahata, K., Kato, M., Kitamura, N., and Komada, M. (2003). STAM proteins bind ubiquitinated proteins on the early endosome via the VHS domain and ubiquitin-interacting motif. Mol Biol Cell 14, 3675-3689.

Mizuno, E., Kawahata, K., Okamoto, A., Kitamura, N., and Komada, M. (2004). Association with Hrs is required for the early endosomal localization, stability, and function of STAM. J Biochem 135, 385-396.

Mizuno, E., Kitamura, N., and Komada, M. (2007). 14-3-3-dependent inhibition of the deubiquitinating activity of UBPY and its cancellation in the M phase. Exp Cell Res 313, 3624-3634.

Mizuno, E., Kobayashi, K., Yamamoto, A., Kitamura, N., and Komada, M. (2006). A deubiquitinating enzyme UBPY regulates the level of protein ubiquitination on endosomes. Traffic 7, 1017-1031.

Mukai, A., Mizuno, E., Kobayashi, K., Matsumoto, M., Nakayama, K.I., Kitamura, N., and Komada, M. (2008). Dynamic regulation of ubiquitylation and deubiquitylation at the central spindle during cytokinesis. J Cell Sci 121, 1325-1333.

Mukai, A., Yamamoto-Hino, M., Awano, W., Watanabe, W., Komada, M., and Goto, S. (2010). Balanced ubiquitylation and deubiquitylation of Frizzled regulate cellular responsiveness to Wg/Wnt. EMBO J 29, 2114-2125.

Nakamura, M., Tanaka, N., Kitamura, N., and Komada, M. (2006). Clathrin anchors deubiquitinating enzymes, AMSH and AMSH-like protein, on early endosomes. Genes Cells 11, 593-606.

Niendorf, S., Oksche, A., Kisser, A., Lohler, J., Prinz, M., Schorle, H., Feller, S., Lewitzky, M., Horak, I., and Knobeloch, K.P. (2007). Essential role of ubiquitin-specific protease 8 for receptor tyrosine kinase stability and endocytic trafficking in vivo. Mol Cell Biol 27, 5029-5039.

Oh, Y.M., Lee, S.B., Choi, J., Suh, H.Y., Shim, S., Song, Y.J., Kim, B., Lee, J.M., Oh, S.J., Jeong, Y., et al. (2014). USP8 modulates ubiquitination of LRIG1 for Met degradation. Sci Rep 4, 4980.

Ohnishi, S., Tochio, N., Tomizawa, T., Akasaka, R., Harada, T., Seki, E., Sato, M., Watanabe, S., Fujikura, Y., Koshiba, S., et al. (2008). Structural basis for controlling the dimerization and stability of the WW domains of an atypical subfamily. Protein Sci 17, 1531-1541.

Johnson, D.R., Bhatnagar, R.S., Knoll, L.J., and Gordon, J.I. (1994). Genetic and biochemical studies of protein N-myristoylation. Annu Rev Biochem 63, 869-914.

Jumper, J., Evans, R., Pritzel, A., Green, T., Figurnov, M., Ronneberger, O., Tunyasuvunakool, K., Bates, R., Žídek, A., Potapenko, A., et al. (2021). Highly accurate protein structure prediction with AlphaFold. Nature 596, 583-589.

Peña-Llopis, S., Vega-Rubín-de-Celis, S., Liao, A., Leng, N., Pavía-Jiménez, A., Wang, S., Yamasaki, T., Zhrebker, L., Sivanand, S., Spence, P., et al. (2012). BAP1 loss defines a new class of renal cell carcinoma. Nat Genet 44, 751-759.

Perez-Rivas, L.G., Theodoropoulou, M., Ferrau, F., Nusser, C., Kawaguchi, K., Stratakis, C.A., Faucz, F.R., Wildemberg, L.E., Assie, G., Beschorner, R., et al. (2015). The Gene of the Ubiquitin-Specific Protease 8 Is Frequently Mutated in Adenomas Causing Cushing's Disease. J Clin Endocrinol Metab 100, E997-1004.

Petosa, C., Masters, S.C., Bankston, L.A., Pohl, J., Wang, B., Fu, H., and Liddington, R.C. (1998). 14-3-3zeta binds a phosphorylated Raf peptide and an unphosphorylated peptide via its conserved amphipathic groove. J Biol Chem 273, 16305-16310.

Qin, X., Wang, R., Xu, H., Tu, L., Chen, H., Li, H., Liu, N., Wang, J., Li, S., Yin, F., et al. (2022). Identification of an autoinhibitory, mitophagy-inducing peptide derived from the transmembrane domain of USP30. Autophagy 18, 2178-2197.

Rabl, J., Bunker, R.D., Schenk, A.D., Cavadini, S., Gill, M.E., Abdulrahman, W., Andrés-Pons, A., Luijsterburg, M.S., Ibrahim, A.F.M., Branigan, E., et al. (2019). Structural Basis of BRCC36 Function in DNA Repair and Immune Regulation. Mol Cell 75, 483-497.e489.

Reincke, M., Sbiera, S., Hayakawa, A., Theodoropoulou, M., Osswald, A., Beuschlein, F., Meitinger, T., Mizuno-Yamasaki, E., Kawaguchi, K., Saeki, Y., et al. (2015). Mutations in the deubiquitinase gene USP8 cause Cushing's disease. Nat Genet 47, 31-38.

Renatus, M., Parrado, S.G., D'Arcy, A., Eidhoff, U., Gerhartz, B., Hassiepen, U., Pierrat, B., Riedl, R., Vinzenz, D., Worpenberg, S., et al. (2006). Structural basis of ubiquitin recognition by the deubiquitinating protease USP2. Structure 14, 1293-1302.

Rougé, L., Bainbridge, T.W., Kwok, M., Tong, R., Di Lello, P., Wertz, I.E., Maurer, T., Ernst, J.A., and Murray, J. (2016). Molecular Understanding of USP7 Substrate Recognition and C-Terminal Activation. Structure 24, 1335-1345.

Row, P.E., Liu, H., Hayes, S., Welchman, R., Charalabous, P., Hofmann, K., Clague, M.J., Sanderson, C.M., and Urbe, S. (2007). The MIT domain of UBPY constitutes a CHMP binding and endosomal localization signal required for efficient epidermal growth factor receptor degradation. J Biol Chem 282, 30929-30937.

Row, P.E., Prior, I.A., McCullough, J., Clague, M.J., and Urbe, S. (2006). The ubiquitin isopeptidase UBPY regulates endosomal ubiquitin dynamics and is essential for receptor down-regulation. J Biol Chem 281, 12618-12624.

Sahtoe, D.D., van Dijk, W.J., El Oualid, F., Ekkebus, R., Ovaa, H., and Sixma, T.K. (2015). Mechanism of UCH-L5 activation and inhibition by DEUBAD domains in RPN13 and INO80G. Mol Cell 57, 887-900.

Salah, Z., Alian, A., and Aqeilan, R.I. (2012). WW domain-containing proteins: retrospectives and the future. Front Biosci (Landmark Ed) 17, 331-348.

Sato, Y., Yoshikawa, A., Yamagata, A., Mimura, H., Yamashita, M., Ookata, K., Nureki, O., Iwai, K., Komada, M., and Fukai, S. (2008). Structural basis for specific cleavage of Lys 63-linked polyubiquitin chains. Nature 455, 358-362.

Sauer, F., Klemm, T., Kollampally, R.B., Tessmer, I., Nair, R.K., Popov, N., and Kisker, C. (2019). Differential Oligomerization of the Deubiquitinases USP25 and USP28 Regulates Their Activities. Mol Cell 74, 421-435 e410.

Schlicher, L., Wissler, M., Preiss, F., Brauns-Schubert, P., Jakob, C., Dumit, V., Borner, C., Dengjel, J., and Maurer, U. (2016). SPATA2 promotes CYLD activity and regulates TNF-induced NF-kappaB signaling and cell death. EMBO Rep 17, 1485-1497.

Shahriyar, S.A., Woo, S.M., Seo, S.U., Min, K.J., and Kwon, T.K. (2018). Cepharanthine Enhances TRAIL-Mediated Apoptosis Through STAMBPL1-Mediated Downregulation of Survivin Expression in Renal Carcinoma Cells. Int J Mol Sci 19.

Solomons, J., Sabin, C., Poudevigne, E., Usami, Y., Hulsik, D.L., Macheboeuf, P., Hartlieb, B., Göttlinger, H., and Weissenhorn, W. (2011). Structural basis for ESCRT-III CHMP3 recruitment of AMSH. Structure 19, 1149-1159.

Swatek, K.N., and Komander, D. (2016). Ubiquitin modifications. Cell Res 26, 399-422.

Takata, H., Kato, M., Denda, K., and Kitamura, N. (2000). A hrs binding protein having a Src homology 3 domain is involved in intracellular degradation of growth factors and their receptors. Genes Cells 5, 57-69.

Thinon, E., Serwa, R.A., Broncel, M., Brannigan, J.A., Brassat, U., Wright, M.H., Heal, W.P., Wilkinson, A.J., Mann, D.J., and Tate, E.W. (2014). Global profiling of co- and post-translationally N-myristoylated proteomes in human cells. Nat Commun 5, 4919.

Treppiedi, D., Barbieri, A.M., Di Muro, G., Marra, G., Mangili, F., Catalano, R., Esposito, E., Ferrante, E., Serban, A.L., Locatelli, M., et al. (2021). Genetic Profiling of a Cohort of Italian

Patients with ACTH-Secreting Pituitary Tumors and Characterization of a Novel. Cancers (Basel) 13.

Tsang, H.T., Connell, J.W., Brown, S.E., Thompson, A., Reid, E., and Sanderson, C.M. (2006). A systematic analysis of human CHMP protein interactions: additional MIT domain-containing proteins bind to multiple components of the human ESCRT III complex. Genomics 88, 333-346.

Tse, W.K., Eisenhaber, B., Ho, S.H., Ng, Q., Eisenhaber, F., and Jiang, Y.J. (2009). Genome-wide loss-of-function analysis of deubiquitylating enzymes for zebrafish development. BMC Genomics 10, 637.

Tsou, W.L., Sheedlo, M.J., Morrow, M.E., Blount, J.R., McGregor, K.M., Das, C., and Todi, S.V. (2012). Systematic analysis of the physiological importance of deubiquitinating enzymes. PLoS One 7, e43112.

Tunyasuvunakool, K., Adler, J., Wu, Z., Green, T., Zielinski, M., Žídek, A., Bridgland, A., Cowie, A., Meyer, C., Laydon, A., et al. (2021). Highly accurate protein structure prediction for the human proteome. Nature 596, 590-596.

Turnbull, A.P., Ioannidis, S., Krajewski, W.W., Pinto-Fernandez, A., Heride, C., Martin, A.C.L., Tonkin, L.M., Townsend, E.C., Buker, S.M., Lancia, D.R., et al. (2017). Molecular basis of USP7 inhibition by selective small-molecule inhibitors. Nature 550, 481-486.

Udenwobele, D.I., Su, R.C., Good, S.V., Ball, T.B., Varma Shrivastav, S., and Shrivastav, A. (2017). Myristoylation: An Important Protein Modification in the Immune Response. Front Immunol 8, 751. 10.3389/fimmu.2017.00751.

Vere, G., Kealy, R., Kessler, B.M., and Pinto-Fernandez, A. (2020). Ubiquitomics: An Overview and Future. Biomolecules 10.

Verspurten, J., Gevaert, K., Declercq, W., and Vandenabeele, P. (2009). SitePredicting the cleavage of proteinase substrates. Trends Biochem Sci 34, 319-323.

Wagner, S.A., Satpathy, S., Beli, P., and Choudhary, C. (2016). SPATA2 links CYLD to the TNF-alpha receptor signaling complex and modulates the receptor signaling outcomes. EMBO J 35, 1868-1884.

Walden, M., Tian, L., Ross, R.L., Sykora, U.M., Byrne, D.P., Hesketh, E.L., Masandi, S.K., Cassel, J., George, R., Ault, J.R., et al. (2019). Metabolic control of BRISC-SHMT2 assembly regulates immune signalling. Nature 570, 194-199.

Wang, D., Xu, C., Yang, W., Chen, J., Ou, Y., Guan, Y., Guan, J., and Liu, Y. (2022). E3 ligase RNF167 and deubiquitinase STAMBPL1 modulate mTOR and cancer progression. Mol Cell 82, 770-784.e779.

Wang, Y., Jiang, Y., Ding, S., Li, J., Song, N., Ren, Y., Hong, D., Wu, C., Li, B., Wang, F., et al. (2018). Small molecule inhibitors reveal allosteric regulation of USP14 via steric blockade. Cell Res 28, 1186-1194.

Williams, R.L., and Urbé, S. (2007). The emerging shape of the ESCRT machinery. Nat Rev Mol Cell Biol 8, 355-368.

Wu, X., Yen, L., Irwin, L., Sweeney, C., and Carraway, K.L., 3rd (2004). Stabilization of the E3 ubiquitin ligase Nrdp1 by the deubiquitinating enzyme USP8. Mol Cell Biol 24, 7748-7757.

Xia, R., Jia, H., Fan, J., Liu, Y., and Jia, J. (2012). USP8 promotes smoothened signaling by preventing its ubiquitination and changing its subcellular localization. PLoS Biol 10, e1001238.

Xue, W., Zhang, S.X., He, W.T., Hong, J.Y., Jiang, L.L., and Hu, H.Y. (2020). Domain interactions reveal auto-inhibition of the deubiquitinating enzyme USP19 and its activation by HSP90 in the modulation of huntingtin aggregation. Biochem J 477, 4295-4312.

Ye, Y., Scheel, H., Hofmann, K., and Komander, D. (2009). Dissection of USP catalytic domains reveals five common insertion points. Mol Biosyst 5, 1797-1808.

Yin, J., Schoeffler, A.J., Wickliffe, K., Newton, K., Starovasnik, M.A., Dueber, E.C., and Harris, S.F. (2015). Structural Insights into WD-Repeat 48 Activation of Ubiquitin-Specific Protease 46. Structure 23, 2043-2054.

Yu, D.J., Qian, J., Jin, X., Li, J., Guo, C.X., and Yue, X.C. (2019). STAMBPL1 knockdown has antitumour effects on gastric cancer biological activities. Oncol Lett 18, 4421-4428.

Zheng, N., and Shabek, N. (2017). Ubiquitin Ligases: Structure, Function, and Regulation. Annu Rev Biochem 86, 129-157.

Zheng, Q., Li, G., Wang, S., Zhou, Y., Liu, K., Gao, Y., Zheng, L., Zhu, L., Deng, Q., Wu, M., et al. (2021). Trisomy 21-induced dysregulation of microglial homeostasis in Alzheimer's brains is mediated by USP25. Sci Adv 7.

Zhou, Q., Yu, X., Demirkaya, E., Deuitch, N., Stone, D., Tsai, W.L., Kuehn, H.S., Wang, H., Yang, D., Park, Y.H., et al. (2016). Biallelic hypomorphic mutations in a linear deubiquitinase define otulipenia, an early-onset autoinflammatory disease. Proc Natl Acad Sci U S A 113, 10127-10132.

Asamizu, K. (2018). Master Thesis.

Kubo, M. (2018). Master Thesis.

Inoko, K. (2018). Master Thesis.

6. Achievements

Presentations

- *New Frontier for Ubiquitin Biology Driven by Chemo-technologies 2nd Ubiquitin Symposium, Tokyo, Japan*: The autoinhibitory regulation of ubiquitin-specific protease 8. **Kakihara, K.**, Asamizu, K., Endo, A., Komada, M., Fukushima, T., 2019.
- *Japanese Biochemical Society Kanto Branch Regular Meeting, Yokohama, Japan*: The autoinhibitory regulation of ubiquitin-specific protease 8. **Kakihara, K.**, Asamizu, K., Endo, A., Komada, M., Fukushima, T., 2019.
- *Japanese Biochemical Society Annual Meeting, Yokohama, Japan*: A novel autoinhibitory mechanism of ubiquitin-specific protease 8 activity via the intramolecular interaction. **Kakihara, K.**, Asamizu, K., Endo, A., Komada, M., Fukushima, T., 2019.
- *American Society for Cell Biology and European Molecular Biology Organization Joint Meeting, D.C., US*: The enzyme activity of ubiquitin-specific protease 8 is regulated by the intramolecular interaction of the USP domain and the WW domain. **Kakihara, K.**, Asamizu, K., Endo, A., Komada, M., Fukushima, T., 2019.
- *New Frontier for Ubiquitin Biology Driven by Chemo-technologies 3rd Ubiquitin Symposium, Chiba, Japan*: The enzyme activity of ubiquitin-specific protease 8 is regulated by the intramolecular interaction of the USP Domain and the WW Domain. **Kakihara, K.**, Asamizu, K., Endo, A., Moritsugu, K., Kato, A., Komada, M., Fukushima, T., 2019.
- *Japanese Society for Virology Annual Meeting, Kobe, Japan*: Recruitment of viral RNA into lentivirus particles is facilitated by GAG ubiquitination. Himi, Y., **Kakihara, K.**, Kato, A., Komada, M., Fukushima, T., 2021.
- *New Frontier for Ubiquitin Biology Driven by Chemo-technologies 3rd Young Researchers Meeting, Online*: Molecular basis of USP8 autoinhibition by WW-like domain. **Kakihara, K.**, 2021.
- *Molecular Biology Society of Japan Annual Meeting, Yokohama, Japan*: Autoinhibition of USP8 by WW-like domain and the dysregulation in Cushing's disease. **Kakihara, K.**, Asamizu, K., Moritsugu, K., Kitaguchi, T., Endo, A., Kidera, A., Ikeguchi, M., Komada, M., Fukushima, T., 2021.
- *Molecular Biology Society of Japan Annual Meeting, Yokohama, Japan*: USP8 prevents viral replication by inhibiting recruitment of viral RNA into lentivirus particles. Himi, Y., **Kakihara, K.**, Kato, A., Komada, M., Fukushima, T., 2021.
- *New Frontier for Ubiquitin Biology Driven by Chemo-technologies 4th Young Researchers Meeting, Online*: Analysis of a somatic mutation newly identified in WW-like domain of USP8. **Kakihara, K.**, 2022.
- *Japanese Society for Proteases in Pathophysiology Annual Meeting, Ehime, Japan*: Pathogenesis of Cushing's disease by *USP8* mutations. Fukushima, T., **Kakihara, K.**, Komada, M., 2022.
- *European Molecular Biology Organization (EMBO) Workshop, Cavtat, Croatia*: Autoinhibition of USP8 by WW-like domain and the dysregulation in Cushing's disease. **Kakihara, K.**, Moritsugu, K., Kitaguchi, T., Endo, A., Komada, M., Fukushima, T., 2022.
- *Japanese Biochemical Society Annual Meeting, Nagoya, Japan*: Mechanisms of USP8 overactivation causing Cushing's disease. Fukushima, T., **Kakihara, K.**, Asamizu, K., Moritsugu, K., Kitaguchi, T., Komada, M., 2022
- *Molecular Biology Society of Japan Annual Meeting, Chiba, Japan*: Deubiquitination of VAMP8 by USP8 and its role in cytokinesis. Nishioka, Y., **Kakihara, K.**, Endo, A., Komada, M., Fukushima, T., 2022.
- *Ubiquitin New Frontier International Symposium, Tokyo*: Caspase-dependent STAMBPL1 cleavage promotes cell death through its C-terminal fragment with hyperactive deubiquitinating activity. **Kakihara, K.**, Lestari, B., Komada, M., Fukushima, T., 2022.
- *Ubiquitin New Frontier International Symposium, Tokyo*: Molecular mechanisms underlying the over-activation of deubiquitinating enzyme USP8 and USP48 by Cushing's disease-associated mutations. Ando, G., **Kakihara, K.**, Komada, M., Fukushima, T., 2022.
- *Tokyo Metropolitan Institute of Medical Science International Symposium, Tokyo*: *Cis*-activity regulation of USP8 and STAMBPL1, two endosomal deubiquitinating enzymes, and role of dysregulation in disease onset. **Kakihara, K.**, 2022.

Publication

- **Keijun Kakihara**, Kengo Asamizu, Kei Moritsugu, Masahide Kubo, Tetsuya Kitaguchi, Akinori Endo, Akinori Kidera, Mitsunori Ikeguchi, Akira Kato, Masayuki Komada & Toshiaki Fukushima. Molecular basis of ubiquitin-specific protease 8 autoinhibition by the WW-like domain. *Communications Biology* **4**, 1272 (2021).

7. Acknowledgement

I thank Dr. Masayuki Komada, Dr. Toshiaki Fukushima, Dr. Kei Moritsugu, Dr. Tetsuya Kitaguchi, and Dr. Naonobu Fujita for their kind supervision and helpful discussions. I also acknowledge the help of the Biomaterials Analysis Division (Tokyo Institute of Technology) with DNA sequencing analysis. Finally, I appreciate all lab members in Komada Lab sincerely. This work was supported by JSPS KAKENHI Grant Number 22J13915 to me; JSPS KAKENHI Grant Number 17K08625, 19H05289 and 21H00276 to Dr. Fukushima; JSPS KAKENHI Grant Number 15H04293 and JP21H02474 to Dr. Komada; AMED Grant Number JP201m0203004j0002, JP211m0203004j0005 and JP22ym0126806j0001 to Dr. Fukushima and the Nagase Science and Technology Foundation.

8. Table and Figures

Table.1 Selected DUBs with gain/loss-of-function mutations in human disease

Family	DUB	Type of mutation	Related disease
OTU	A20	Loss-of-function	Autoinflammatory syndrome, familial, Behcet-like
	OTUD7A	Loss-of-function	Specific learning disability
	OTUD5	Loss-of-function	Multiple congenital anomalies-neurodevelopmental syndrome, X-linked
	OTUD6B	Loss-of-function	Intellectual developmental disorder with dysmorphic facies, seizures, and distal limb anomalies
	OTULIN	Loss-of-function	Autoinflammation, panniculitis, and dermatosis syndrome
USP	USP8	Gain-of-function	Cushing's disease
	USP48	Gain-of-function	Cushing's disease
	USP6	Gain-of-function	Pseudosarcomatous fibromatosis (promoter-swapping gene fusion)
	USP16	Gain-of-function	Down syndrome (gene triplication)
	USP25	Gain-of-function	Down syndrome (gene triplication)
	USP2	Gain-of-function	Ovarian serous cystadenocarcinoma (overexpression, MLL fusion)
	USP1	Loss-of-function	Fanconi anemia, complementation group a
	USP7	Loss-of-function	Hao-Fountain syndrome
	USP9X	Loss-of-function	Intellectual developmental disorder, X-linked 99
	USP14	Loss-of-function	Autosomal dominant cerebellar ataxia
	USP18	Loss-of-function	Pseudo-Torch syndrome 2
	USP26	Loss-of-function	Male infertility
	USP34	Loss-of-function	Chromosome 2p16.1-p15 deletion syndrome
	USP44	Loss-of-function	Embryonal carcinoma
	USP45	Loss-of-function	Leber congenital amaurosis 19
	CYLD	Loss-of-function	Brooke-Spiegler syndrome
JAMM	STAMBP	Loss-of-function	Microcephaly-capillary malformation syndrome
	MYSM1	Loss-of-function	Bone marrow failure syndrome 4
	BRCC36	Loss-of-function	Moyamoya disease 4 with short stature, hypergonadotropic hypogonadism, and facial dysmorphism
UCH	UCHL1	Gain-of-function	Parkinson disease 5, autosomal dominant (missense mutation (I93M))
	BAP1	Loss-of-function	Bap1 tumor predisposition syndrome

Fig. 1

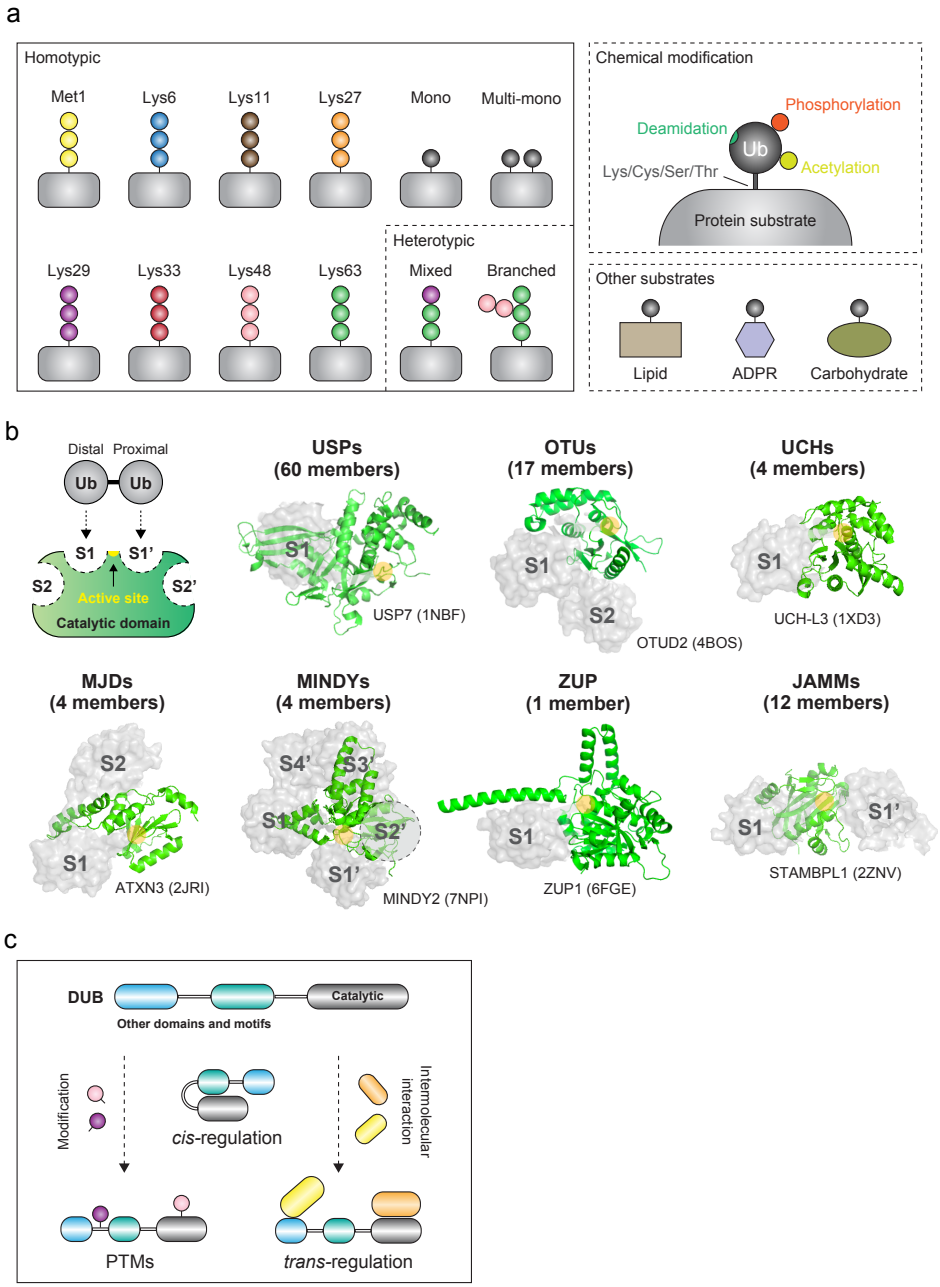
a
Homotypic
Met1
Lys6
Lys11
Lys27
Mono
Multi-mono
Heterotypic
Lys29
Lys33
Lys48
Lys63
Mixed
Branched
Chemical modification
Phosphorylation
Deamidation
Ub
Acetylation
Lys/Cys/Ser/Thr
Protein substrate
Other substrates
Lipid
ADPR
Carbohydrate
b
Distal
Proximal
Ub
Ub
S1
S1'
S2
Active site
S2'
Catalytic domain
USPs
(60 members)
USP7 (1NBF)
OTUs
(17 members)
OTUD2 (4BOS)
UCHs
(4 members)
UCH-L3 (1XD3)
MJDs
(4 members)
ATXN3 (2JRI)
MINDYs
(4 members)
MINDY2 (7NPI)
ZUP
(1 member)
ZUP1 (6FGE)
JAMMs
(12 members)
STAMBPL1 (2ZNV)
c
DUB
Catalytic
Other domains and motifs
Modification
cis-regulation
Intermolecular interaction
PTMs
trans-regulation

Fig. 1 Ubiquitin code and DUB families

a. Types of ubiquitination and chemical modifications to ubiquitin itself. Ubiquitination target is typically a lysine residue of the target protein. Types of ubiquitination can be structurally classified as monoubiquitin, multi-monoubiquitin, homotypic polyubiquitin chain (Met1, Lys6, Lys11, Lys27, Lys29, Lys33, Lys48, and Lys63-linkages), and heterotypic polyubiquitin chains (mixed and branched-linkages). Moreover, novel ubiquitination modalities include new ubiquitination targets (the first-methionine, serine, threonine, and cysteine residues; carbohydrate; lipid; ADP ribose) and the modification of ubiquitin (phosphorylation and acetylation).

b. Distinct catalytic domains in seven DUB families. Representative crystal structure of each DUB family catalytic domains in complex with ubiquitin are shown. DUBs catch the distal ubiquitin into S1 site in their catalytic domain via extensive hydrophobic interactions with ubiquitin. Some DUBs recognize the proximal ubiquitin using S1' site in their catalytic domain. In some cases, they harbor additional ubiquitin-binding sites in their catalytic domain (e.g. S1'-S4' sites in MINDY2; S2 site in OTUD2 and ATXN3). These additional sites are also provided by the other auxiliary domains.

c. *Cis*-, *trans*-regulations and PTMs for tuning DUB activity. Most DUBs are multi-domain proteins including their catalytic domain. Their enzymatic activity is often regulated via PTMs and the trans-regulations via intermolecular interaction with regulatory proteins. Furthermore, some DUBs have the cis-regulations via intramolecular interaction between their intrinsic regulatory and catalytic domains (e.g. autoactivation of USP4; autoinhibition of USP30).

Fig. 2

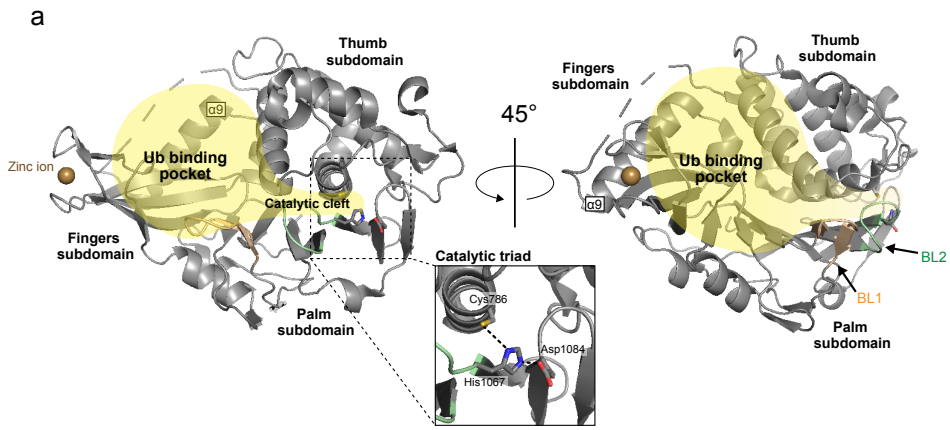

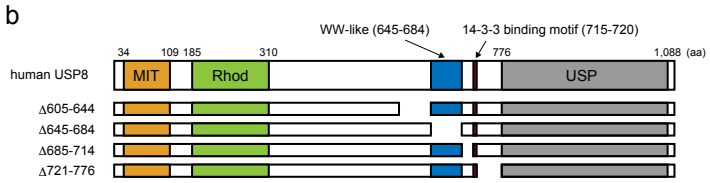

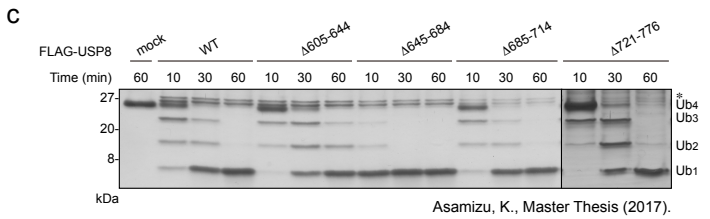

Asamizu, K., Master Thesis (2017).

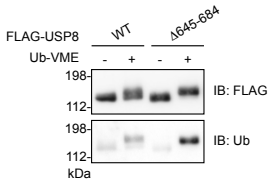

Asamizu, K., Master Thesis (2017).

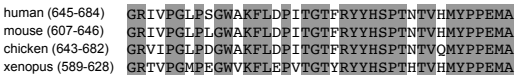

Asamizu, K., Master Thesis (2017).

Asamizu, K., Master Thesis (2017).

Fig. 2 USP8 autoinhibition by its intrinsic WW-like domain

a. Crystal structure of USP8 USP domain (aa. 762–1109; PDB ID: 2GFO). Two representations are rotated by 45° around the Y-axis. The fingers, palm and thumb subdomains are indicated. The catalytic triad formed by Cys786, His1067 and Asp1084 is shown in the enlarged view. The ubiquitin-binding pocket and catalytic cleft are indicated in yellow. The upper-left broken loop between Asp888 and Asn898 is non-structural. BL1, blocking loop 1; BL2, blocking loop 2.

b. Schematic structures of human USP8 and the truncated mutants used in c: MIT, MIT domain; Rhod, rhodanese-like domain; WW-like, WW-like domain; USP, catalytic USP domain.

c. Quantitative DUB assay of USP8 truncated mutants. FLAG-tagged USP8 mutants purified from HEK293T cells were incubated with Lys63-linked ubiquitin tetramers and then subjected to SDA-PAGE and silver-staining. *, copurified protein (s) with USP8.

d. Ubiquitin-vinyl methyl ester (Ub-VME)-labelling of $USP8^{\Delta 645–684}$. FLAG-tagged USP8 mutants purified from HEK293T cells were labelled and subjected to immunoblotting.

e. Sequences showing the autoinhibitory region (aa. 645-684) in USP8 orthologs. Grey highlighting: conserved residues.

f. Sequences similarity of the autoinhibitory region (aa. 645-684) to the atypical WW domains. The arrow indicates the conserved N-terminal tryptophan. The consensus sequence of the WW domain is also shown.

Fig. 3

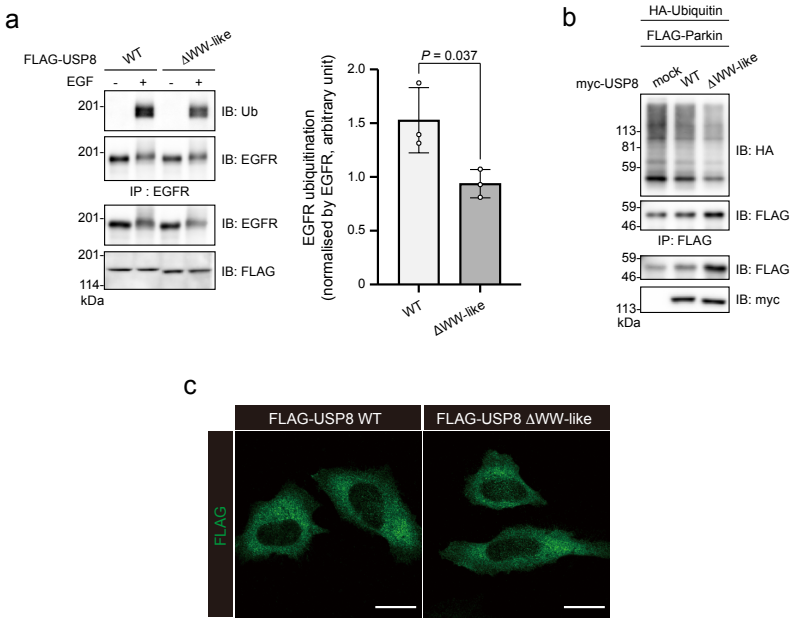

Fig. 3 USP8 autoinhibition by the WW-like domain toward cellular substrates

a. EGFR ubiquitination levels in cells expressing USP8$^{\Delta WW\text{-like}}$. HeLa cells stably expressing FLAG-tagged USP8 mutants were treated with EGF. The lysates were subjected to immunoprecipitation and immunoblotting. The right graph shows EGFR ubiquitination levels normalized by EGFR in the immunoprecipitates.

b. Parkin ubiquitination levels in cells overexpressing USP8$^{\Delta WW\text{-like}}$. HEK293T cells overexpressing myc-tagged USP8 mutants, FLAG-tagged Parkin, and HA-tagged ubiquitin were lysed. The lysates were subjected to immunoprecipitation and immunoblotting.

c. Cellular localization of USP8$^{\Delta WW\text{-like}}$. HeLa cells expressing FLAG-tagged USP8 mutants were fixed and stained for confocal microscopy observations. Scale bars, 20 mm.

The graph shows the means ± standard deviations of three independent experiments. Statistical significance was determined using Student's t-test.

Fig. 4

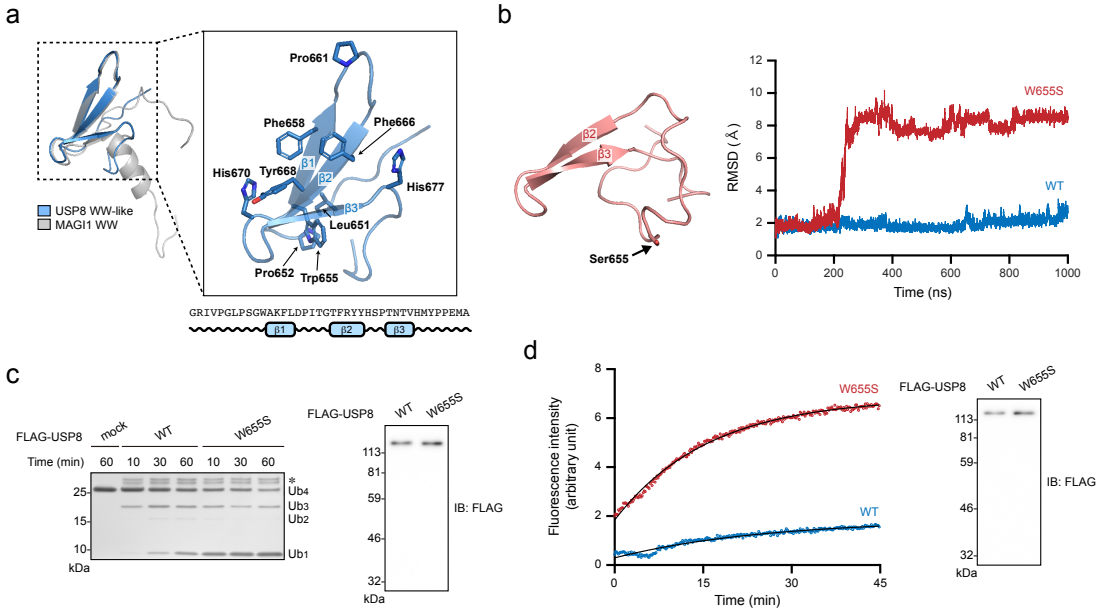

Fig. 4 Structural modelling of USP8 WW-like domain.

a. Structural model of the WW-like domain. Left, superposition of the predicted model (blue) and MAGI1 WW domain (grey) as well as the secondary structure based on the model. Right, magnification of the hydrophobic surface formed by three antiparallel β-sheets.

b. Molecular dynamics (MD) simulations of the predicted model and Trp655 to Ser (W655S) mutant. Left, Structural model of the W655S mutant. Right, the root means square deviations (RMSD) from the predicted structure as a function of simulation time. Blue, WT. Red, W655S mutant.

c. Quantitative DUB assay of USP8^{W665S}. FLAG-tagged USP8 mutants purified from HEK293T cells were validated using immunoblotting (right) and incubated with Lys63-linked ubiquitin tetramers (left). Samples were then subjected to SDA-PAGE and silver-staining. *, copurified protein (s) with USP8.

d. Quantitative DUB assay of USP8^{W665S}. FLAG-tagged USP8 mutants purified from HEK293 cells were validated using immunoblotting (right) and incubated with Ub-AMC (left). The released AMC fluorescence was analyzed at the indicated time points.

Fig. 5

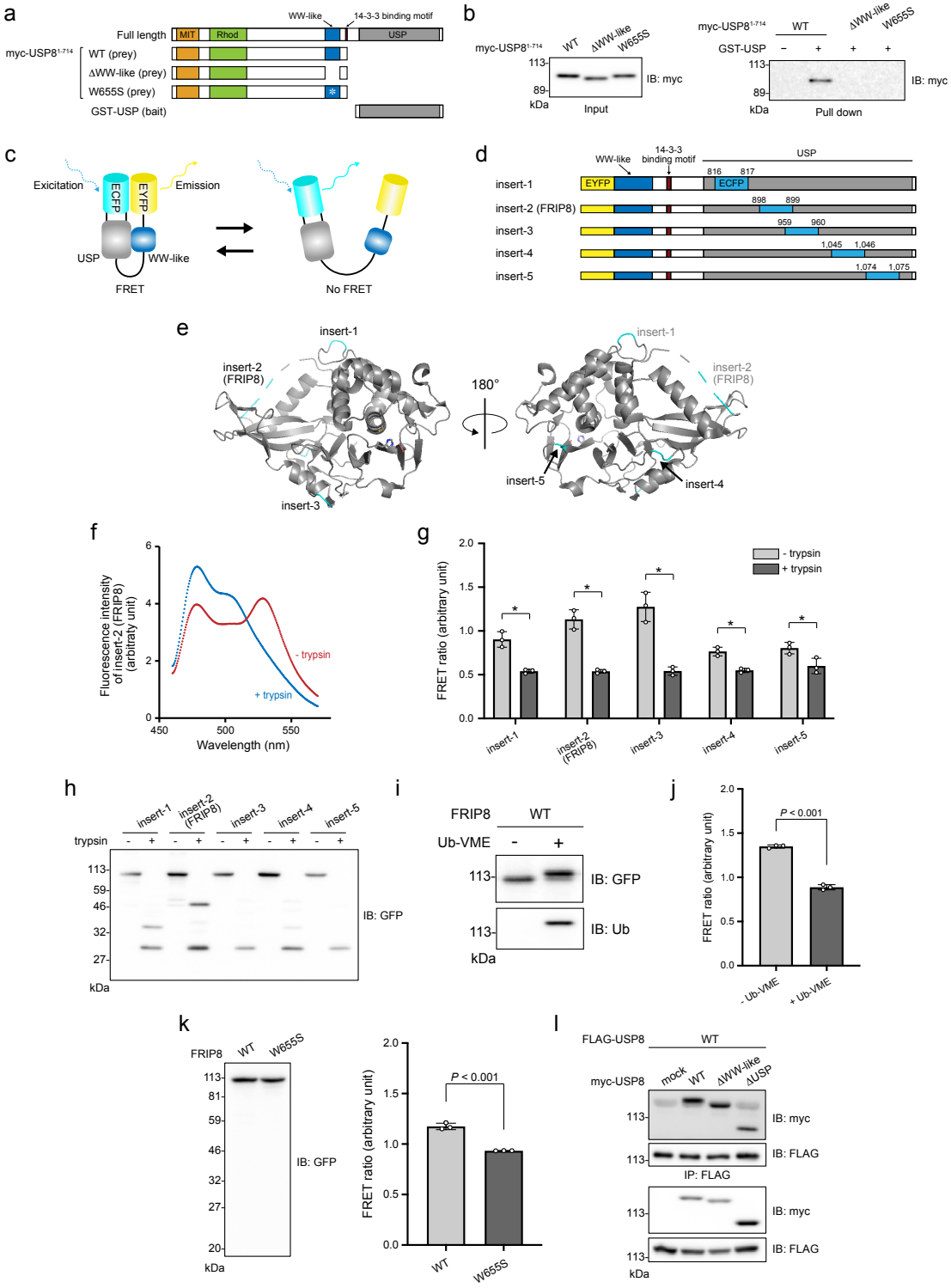
a
WW-like
14-3-3 binding motif
Full length
MIT
Rhod
USP
myc-USP8 1-714
WT (prey)
ΔWW-like (prey)
W655S (prey)
GST-USP (bait)
b
myc-USP8 1-714
WT
ΔWW-like
W655S
113
89
kDa
IB: myc
Input
GST-USP
Pull down
c
Excitation
Emission
ECFP
EYFP
USP
WW-like
FRET
No FRET
d
insert-1
insert-2 (FRIP8)
insert-3
insert-4
insert-5
816
817
898
899
959
960
1,045
1,046
1,074
1,075
e
180°
f
Fluorescence intensity of insert-2 (FRIP8) (arbitraty unit)
- trypsin
+ trypsin
Wavelength (nm)
g
FRET ratio (arbitrary unit)
h
trypsin
IB: GFP
i
FRIP8
Ub-VME
IB: Ub
j
P < 0.001
- Ub-VME
+ Ub-VME
k
W655S
l
FLAG-USP8
mock
ΔUSP
IB: FLAG
IP: FLAG

Fig. 5 Interaction between the WW-like and USP domains

a. Schematic structures of the prey and bait proteins used in b.

b. Interaction of the WW-like domain with the USP domain. Lysates of HEK293T cells overexpressing myc-tagged $USP8^{1–714}$ mutants shown in a were incubated with GST-tagged USP domain, subsequently precipitated using glutathione beads. The adsorbed fraction (right) and input (left) were analyzed using immunoblotting.

c. Schematic representation of single-molecule FRET probes used to detect the interaction.

d. Schematic structures of the probes.

e. ECFP insertion points are depicted on a crystal structure of the USP domain (PDB ID: 2GFO). Two representations are rotated by 180° around the Y-axis.

f. Representative emission spectra of FRET probe at an excitation wavelength of 433 nm. Lysate of HEK293T cells overexpressing insert-2 probe was subjected to FRET assay with (blue) and without (red) trypsinization.

g, h. FRET ratio of probes indicated in d. Lysates of HEK293T cells overexpressing each probe were subjected to fluorescence measurement (FRET assay) (g) and immunoblotting (h) before (light) and after (dark) trypsinization. The ratio of the emission intensity of EYFP to that of ECFP (FRET ratio) was calculated.

i, j. Ub-VME-labelling of FRIP8. His-tagged FRIP8 purified from HEK293T cells was labelled with Ub-VME. The samples were subsequently subjected to immunoblotting (i) and FRET assay (j).

k. Effects of the W655S substitution on the FRET ratio. Lysates of HEK293T cells overexpressing each FRIP8 were subjected to FRET assay (right) and immunoblotting (left).

l. Roles of the WW-like and USP domains in USP8 dimerization. HEK293T cells overexpressing FLAG- or myc-tagged USP8 mutants were lysed, and then subjected to immunoprecipitation and immunoblotting.

The graph shows the means ± standard deviations of three independent experiments. Statistical significance was determined using Student's t-test.

Fig. 6

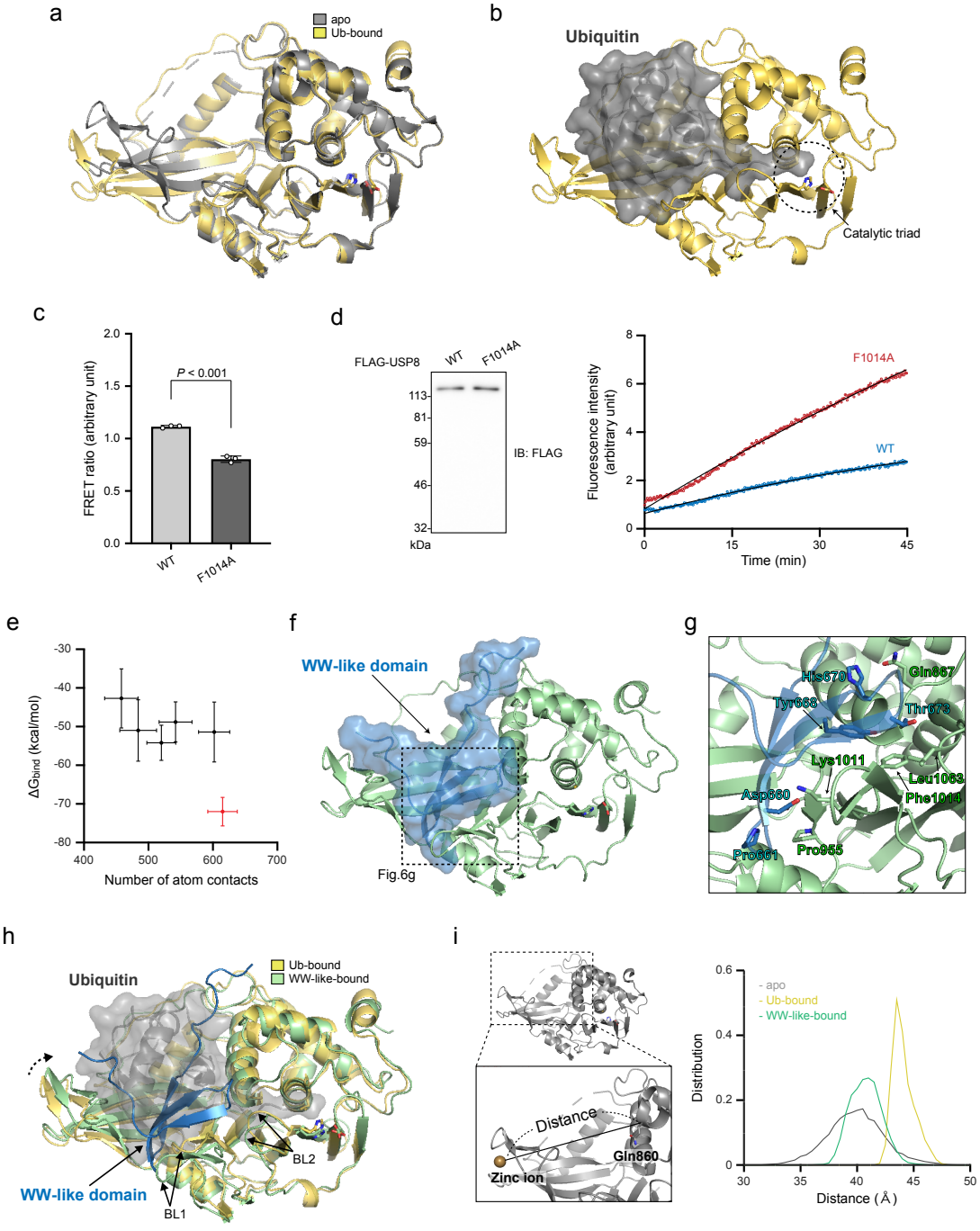
a
apo
Ub-bound
b
Ubiquitin
Catalytic triad
c
FRET ratio (arbitrary unit)
P < 0.001
WT
F1014A
d
FLAG-USP8
WT
F1014A
113-
81-
59-
46-
32-
kDa
IB: FLAG
Fluorescence intensity (arbitrary unit)
F1014A
WT
Time (min)
e
ΔGbind (kcal/mol)
Number of atom contacts
f
WW-like domain
Fig.6g
g
His670
Gln867
Tyr668
Thr673
Lys1011
Leu1063
Asp860
Phe1014
Pro861
Pro855
h
Ubiquitin
Ub-bound
WW-like-bound
BL2
WW-like domain
BL1
i
Distance
Gln860
Zinc ion
- apo
- Ub-bound
- WW-like-bound
Distribution
Distance (Å)

Fig. 6

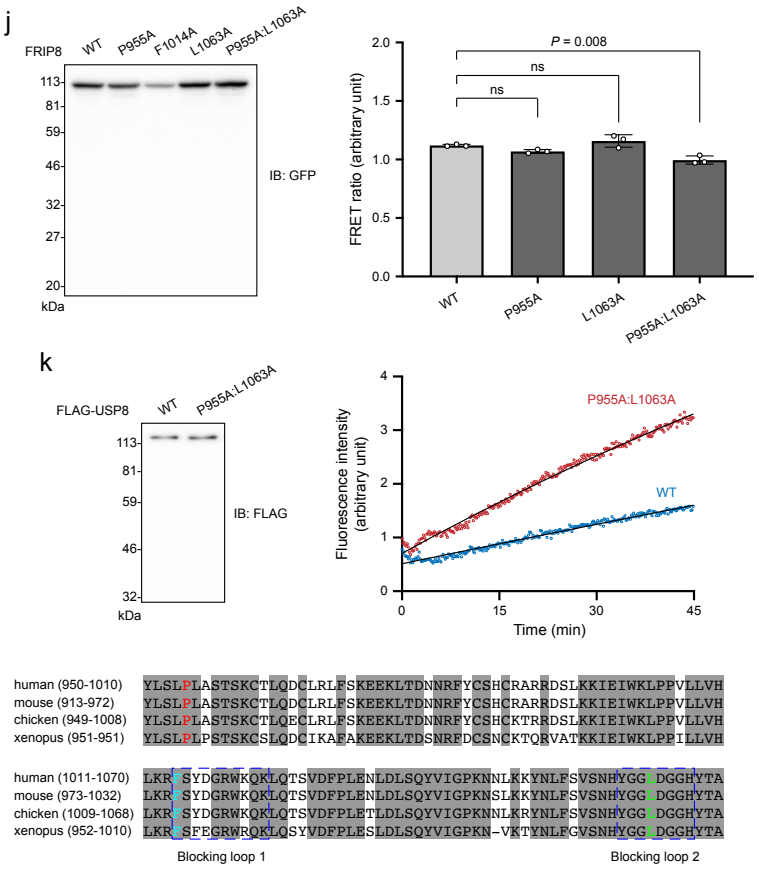
j
FRIP8
WT
P955A
F1014A
L1063A
P955A:L1063A
113
81
59
46
32
27
20
kDa
IB: GFP
FRET ratio (arbitrary unit)
2.0
1.5
1.0
0.5
0.0
P = 0.008
ns
ns
WT
P955A
L1063A
P955A:L1063A
k
FLAG-USP8
WT
P955A:L1063A
113
81
59
46
32
kDa
IB: FLAG
Fluorescence intensity (arbitrary unit)
P955A:L1063A
WT
Time (min)
0
15
30
45
l
human (950-1010) YLSLPLASTSKCTLQDCLRLFSKEEKLTDNNRFYCSHCRARRDSLKKIEIWKLPPVLLVH
mouse (913-972) YLSLPLASTSKCTLQDCLRLFSKEEKLTDNNRFYCSHCRARRDSLKKIEIWKLPPVLLVH
chicken (949-1008) YLSLPLASTSKCTLQECLRLFSKEEKLTDNNRFYCSHCKTRRDSLKKIEIWKLPPVLLVH
xenopus (951-951) YLSLPLPSTSKCSLQDCIKAFAKEEKLTDSNRFDCSNCKTQRVATKKIEIWKLPPILLVH
human (1011-1070) LKRCSYDGRWKQKLQTSVDFPLENLDLSQYVIGPKNNLKKYNLFSVSNHYGGCDGGHYTA
mouse (973-1032) LKRCSYDGRWKQKLQTSVDFPLENLDLSQYVIGPKNSLKKYNLFSVSNHYGGCDGGHYTA
chicken (1009-1068) LKRCSYDGRWKQKLQTSVDFPLETLDLSQYVIGPKNNLKRYNLFSVSNHYGGCDGGHYTA
xenopus (952-1010) LKRCSFEGRWRQKLQSYVDFPLESLDLSQYVIGPKN-VKTYNLFGVSNHYGGCDGGHYTA
Blocking loop 1
Blocking loop 2

Fig. 6 Structural modeling of the WW-like domain in complex with the USP domain

a. Superposition of the two USP domain structures: the ubiquitin-bound form of the present model in b (yellow) and the apo form (PDB ID: 2GFO, grey).

b. Structure model of the USP domain in ubiquitin-bound form. The USP domain and the bound ubiquitin are shown in yellow and grey, respectively.

c. Effects of the F1014A substitution on the FRET ratio. Lysates of HEK293T cells expressing each FRIP8 were subjected to FRET assay (left) and immunoblotting (Fig. 6j).

d. Quantitative DUB assay of $USP8^{F1014A}$. FLAG-tagged USP8 mutants purified from HEK293 cells were validated using immunoblotting (left) and incubated with Ub-AMC (right). The released AMC fluorescence was analyzed at the indicated time points.

e. Number of atom contacts, N_c, and binding free energy, ΔG_{bind}, between the WW-like and USP domains are plotted for six model candidates. The selected model structure with the largest N_c and the lowest ΔG_{bind} is shown in red. See Methods for definition.

f. Complex structure model of the WW-like domain (blue) and USP domain (green), as predicted by docking simulations using the structural models of the WW-like domain presented in Fig. 4a and that of the USP domain presented in Fig. 6b.

g. Close-up view of the contact sites between the WW-like and USP domains.

h. Superposition of the USP domain in the ubiquitin-bound form (yellow) and that in the WW-like domain-bound form (green).

i. Distributions of the distance between zinc ions in the fingers subdomain and Cα atoms of Gln860 during the MD simulations of the WW-like domain-bound (green), ubiquitin-bound (yellow) and apo (grey) forms.

j. Effects of the P955A:L1063A substitution on the FRET ratio. Lysates of HEK293T cells overexpressing each FRIP8 were subjected to FRET assay (right) and immunoblotting (left).

k. Quantitative DUB assay of $USP8^{P955A:L1063A}$. FLAG-tagged USP8 mutants purified from HEK293 cells were validated using immunoblotting (left) and incubated with Ub-AMC (right). The released AMC fluorescence was analyzed at the indicated time points.

l. Sequences showing the conserved residues corresponding to human USP8 Pro955 (red), Phe1014 (blue) and Leu1063 (green) in USP8 orthologs.

The graph shows the means ± standard deviations of three independent experiments. Statistical significance against the WT was determined using one-way ANOVA and Tukey's post-hoc test. ns, not significant.

Fig. 7

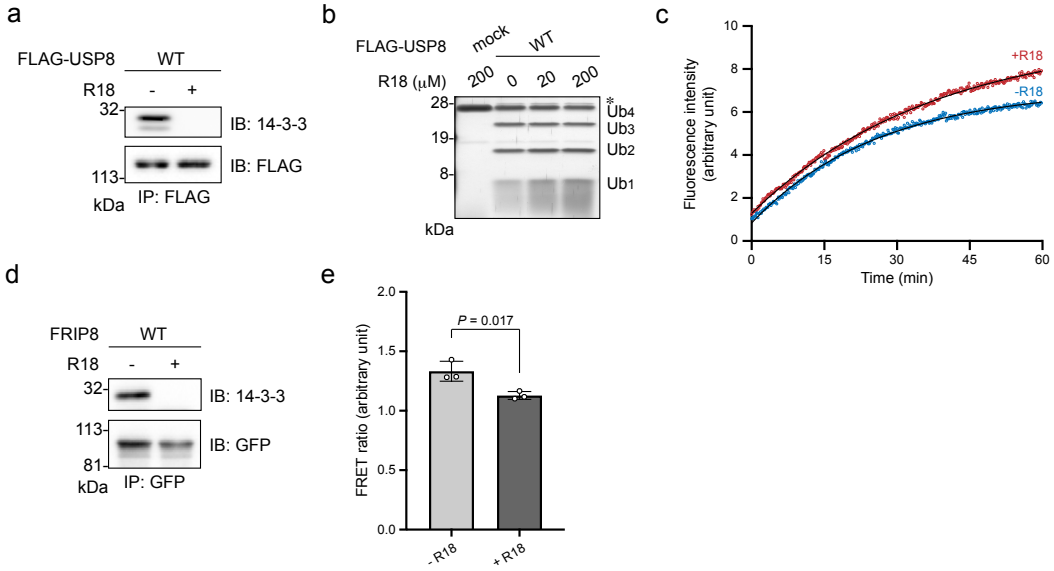

Fig. 7 Enhancement of the autoinhibition by 14-3-3 proteins

a. Effects of R18 peptide on interaction of USP8 with 14-3-3 proteins. HEK293 cells expressing FLAG-tagged USP8 were lysed. The lysate was incubated with 100 μM R18 peptide before immunoprecipitation and immunoblotting.

b, c. Quantitative DUB assay of USP8 with R18 peptide. FLAG-tagged USP8 purified from HEK293 cells were incubated with Lys63-linked ubiquitin tetramers (b) or Ub-AMC (c) in the presence of R18 peptide. Samples were subsequently subjected to silver-staining or fluorescence measurement, respectively.

d, e. Effects of R18 peptide on FRIP8. HEK293 cells expressing FRIP8 and myc-tagged 14-3-3ε were lysed. The lysate was incubated with 100 μM R18 peptide and then subjected to immunoprecipitation, subsequently immunoblotting (d) and FRET assay (e).

The graph shows the means ± standard deviations of three independent experiments. Statistical significance was determined using Student's t-test.

Fig. 8

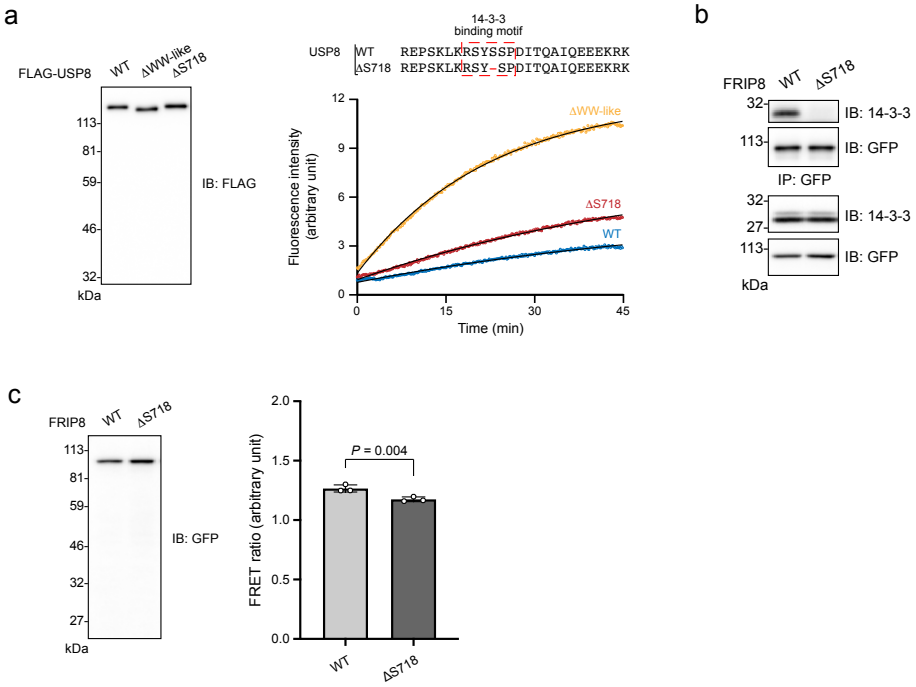

Fig. 8 Relief of the autoinhibition by CD-associated mutation in the 14-3-3-binding motif

a. Quantitative DUB assay of USP8$^{\Delta S718}$. The mutational site is shown in the upper right panel. FLAG-tagged USP8 mutants purified from HEK293 cells were validated using immunoblotting (left) and incubated with Ub-AMC (right). The released AMC fluorescence was analyzed at the indicated time points.

b, c. Effects of Cushing's disease-associated mutation (ΔS718) on FRIP8. HEK293 cells expressing FRIP8 mutants were lysed and subjected to immunoprecipitation. Samples were then analyzed using immunoblotting (b) and FRET assay (c).

The graph shows the means ± standard deviations of three independent experiments. Statistical significance was determined using Student's t-test.

Fig. 9

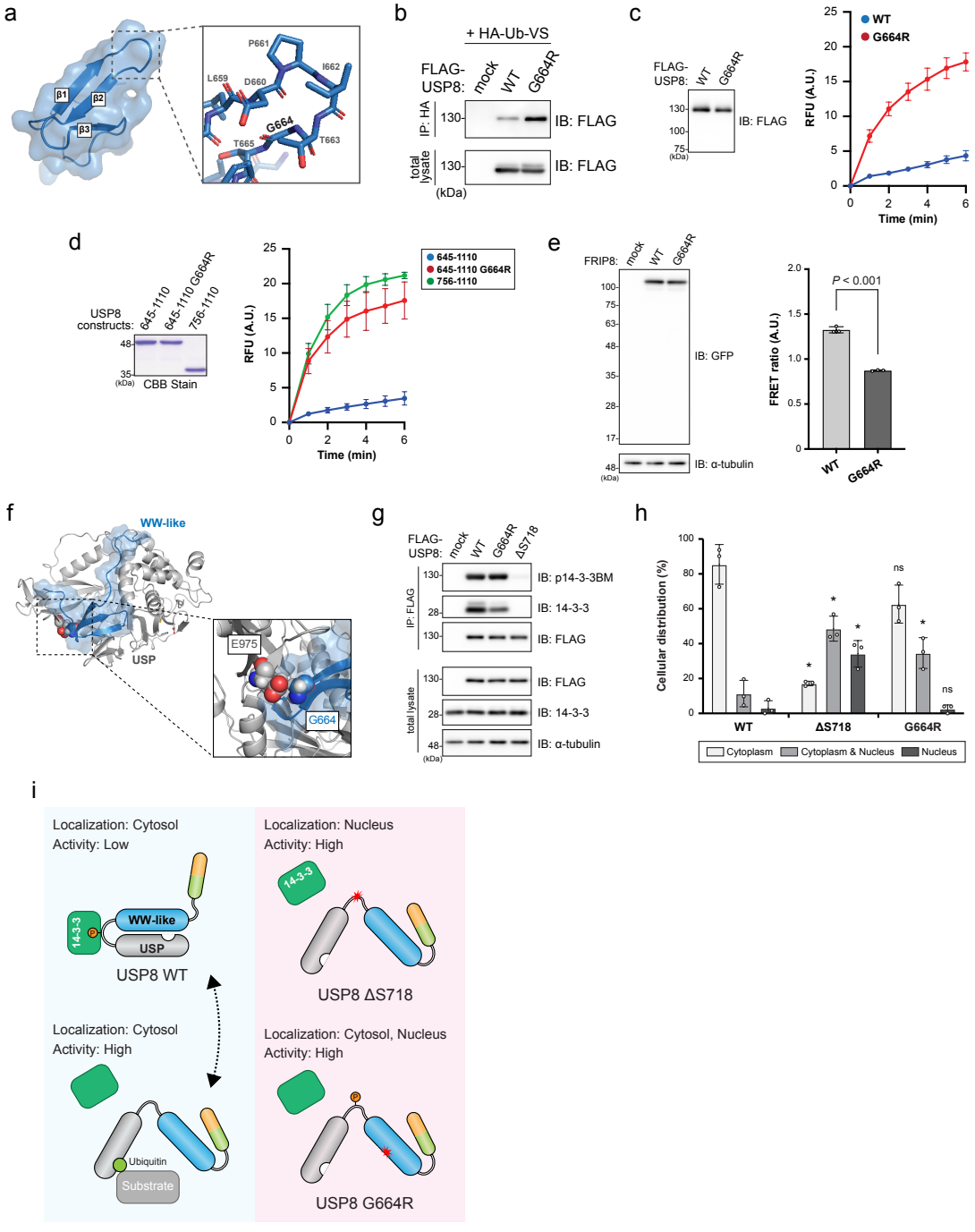
a
β1
β2
β3
P661
I662
L659
D660
G664
T665
T663
b
+ HA-Ub-VS
FLAG-USP8:
mock
WT
G664R
IP: HA
130-
IB: FLAG
total lysate
130-
IB: FLAG
(kDa)
c
FLAG-USP8:
WT
G664R
130-
100-
75-
(kDa)
IB: FLAG
WT
G664R
RFU (A.U.)
Time (min)
d
USP8 constructs:
645-1110
645-1110 G664R
756-1110
48-
35-
(kDa)
CBB Stain
645-1110
645-1110 G664R
756-1110
RFU (A.U.)
Time (min)
e
FRIP8:
mock
WT
G664R
100-
75-
63-
48-
35-
28-
17-
IB: GFP
48-
(kDa)
IB: α-tubulin
FRET ratio (A.U.)
P < 0.001
WT
G664R
f
WW-like
USP
E975
G664
g
FLAG-USP8:
mock
WT
G664R
ΔS718
IP: FLAG
130-
IB: p14-3-3BM
28-
IB: 14-3-3
130-
IB: FLAG
total lysate
130-
IB: FLAG
28-
IB: 14-3-3
48-
(kDa)
IB: α-tubulin
h
Cellular distribution (%)
ns
*
WT
ΔS718
G664R
Cytoplasm
Cytoplasm & Nucleus
Nucleus
i
Localization: Cytosol
Activity: Low
14-3-3
WW-like
USP
USP8 WT
Localization: Nucleus
Activity: High
14-3-3
USP8 ΔS718
Localization: Cytosol
Activity: High
Ubiquitin
Substrate
Localization: Cytosol, Nucleus
Activity: High
USP8 G664R

Fig. 9 Relief of the autoinhibition by CD-associated mutation in the WW-like domain

a. The mutational site of G664R in the structural model of the WW-like domain.

b. HA-tagged ubiquitin-vinyl sulfone (HA-Ub-VS)-labelling of $USP8^{G664R}$. FLAG-tagged USP8 mutants purified from HEK293 cells were labelled and subjected to immunoblotting.

c. Quantitative DUB assay of $USP8^{G664R}$. FLAG-tagged USP8 mutants purified from HEK293 cells were validated using immunoblotting (left) and incubated with Ub-AMC (right). The released AMC fluorescence was analyzed at the indicated time points.

d. Quantitative DUB assay of $USP8^{G664R}$ in the absence of 14-3-3 proteins. GST-tagged USP8 truncated constructs consisting of aa. 645-110 or 756-1110 purified from *E.coli* were validated using immunoblotting (left) and incubated with Ub-AMC (right). The released AMC fluorescence was analyzed at the indicated time points.

e. Effects of Cushing's disease-associated mutation (G664R) on FRIP8. HEK293 cells expressing FRIP8 mutants were lysed. Samples were then analyzed using immunoblotting (left) and FRET assay (right).

f. The mutational site of G664R in the structural model of the WW-like-USP complex.

g. Effects of Cushing's disease-associated mutation (G664R) on the 14-3-3-binding. HEK293 cells expressing FLAG-tagged USP8 mutants were lysed and subjected to immunoprecipitation. Samples were then analyzed using immunoblotting.

h. Effects of Cushing's disease-associated mutations on USP8 cellular localization. HeLa cells overexpressing FLAG-tagged USP8 mutants were fixed and stained for confocal microscopy observations.

i. Working hypothesis of the USP8 autoinhibition and its impairment in Cushing's disease mutants.

The graph shows the means ± standard deviations of three independent experiments. Statistical significance against the WT was determined using one-way ANOVA and Tukey's post-hoc test. ns, not significant.

Fig. 10

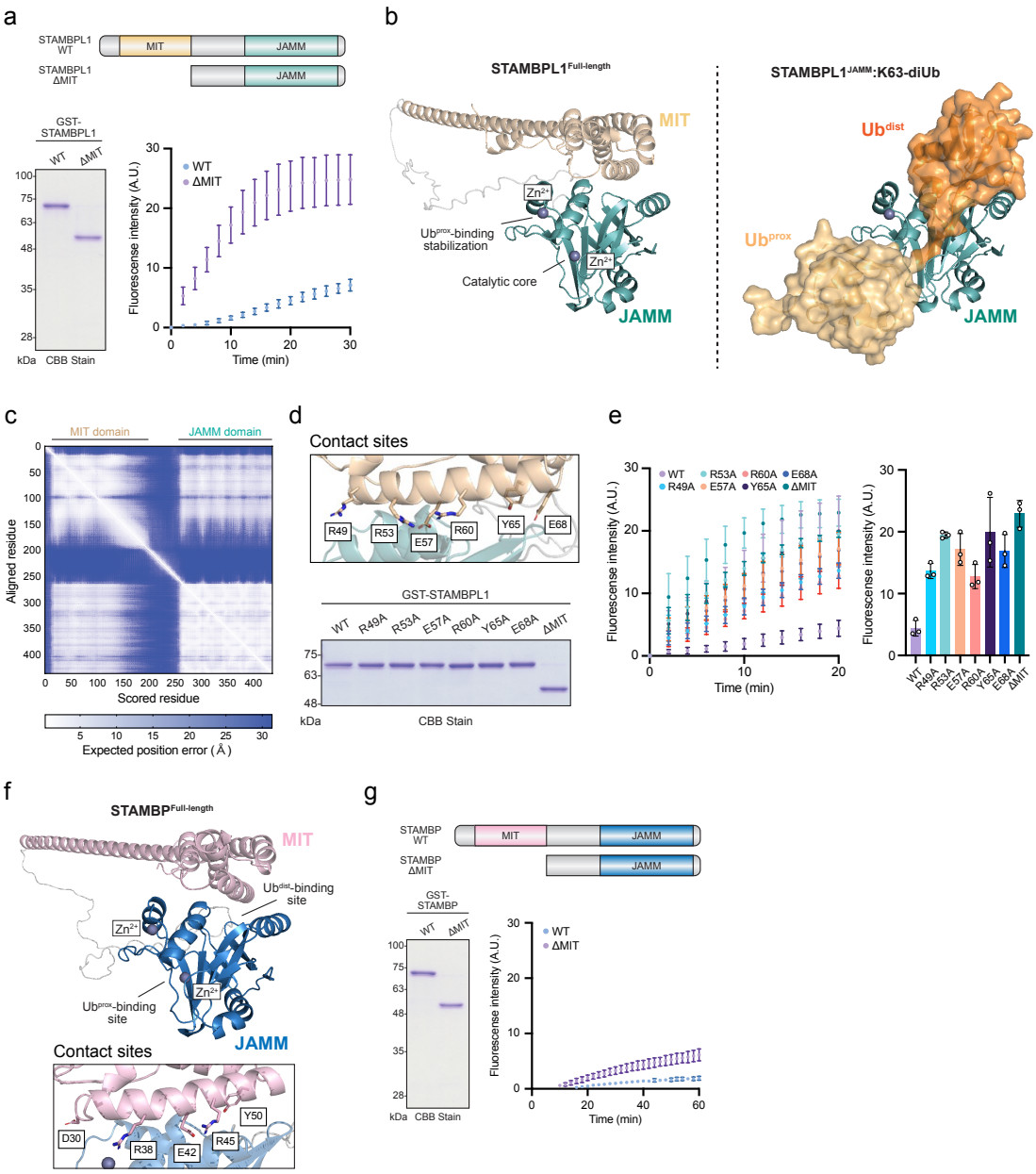
a
STAMBPL1 WT
STAMBPL1 ΔMIT
MIT
JAMM
GST-STAMBPL1
WT
ΔMIT
kDa
CBB Stain
Fluorescense intensity (A.U.)
Time (min)
b
STAMBPL1Full-length
MIT
Zn2+
Ubprox-binding stabilization
Catalytic core
JAMM
STAMBPL1JAMM:K63-diUb
Ubdist
Ubprox
c
MIT domain
JAMM domain
Aligned residue
Scored residue
Expected position error (Å)
d
Contact sites
R49
R53
E57
R60
Y65
E68
GST-STAMBPL1
e
WT
R49A
R53A
E57A
R60A
Y65A
E68A
ΔMIT
Time (min)
f
STAMBPFull-length
Ubdist-binding site
Ubprox-binding site
Contact sites
D30
R38
E42
Y50
R45
g
STAMBP WT
STAMBP ΔMIT
GST-STAMBP

Fig. 10 STAMBPL1 and STAMBP autoinhibition by their intrinsic MIT domain

a. Quantitative DUB assay of STAMBPL1$^{\Delta MIT}$. GST-tagged STAMBPL1 mutants purified from *E.coli* were validated using CBB stain (left) and incubated with Ub-AMC (right). The released AMC fluorescence was analyzed at the indicated time points.

b. Structure model of full-length STAMBPL1 from Alpha Fold2 (left). Crystal structure of STAMBPL1 JAMM domain in complex with Lys63-linked ubiquitin dimer.

c. Predicted aligned error (PAE) score of the full-length STAMBPL1 model. White color shows accuracy of each residue positions.

d, e. Close-up view of the contact sites between the MIT and JAMM domains (d, top). GST-tagged STAMBPL1 mutants purified from *E.coli* were validated using CBB stain (d, bottom) and incubated with Ub-AMC (e). The released AMC fluorescence was analyzed at the indicated time points.

f. Structure model of full-length STAMBP from Alpha Fold2.

g. Quantitative DUB assay of STAMBP$^{\Delta MIT}$. GST-tagged STAMBP mutants purified from *E.coli* were validated using CBB stain (left) and incubated with Ub-AMC (right). The released AMC fluorescence was analyzed at the indicated time points.

The graph shows the means ± standard deviations of three independent experiments.

Fig. 11

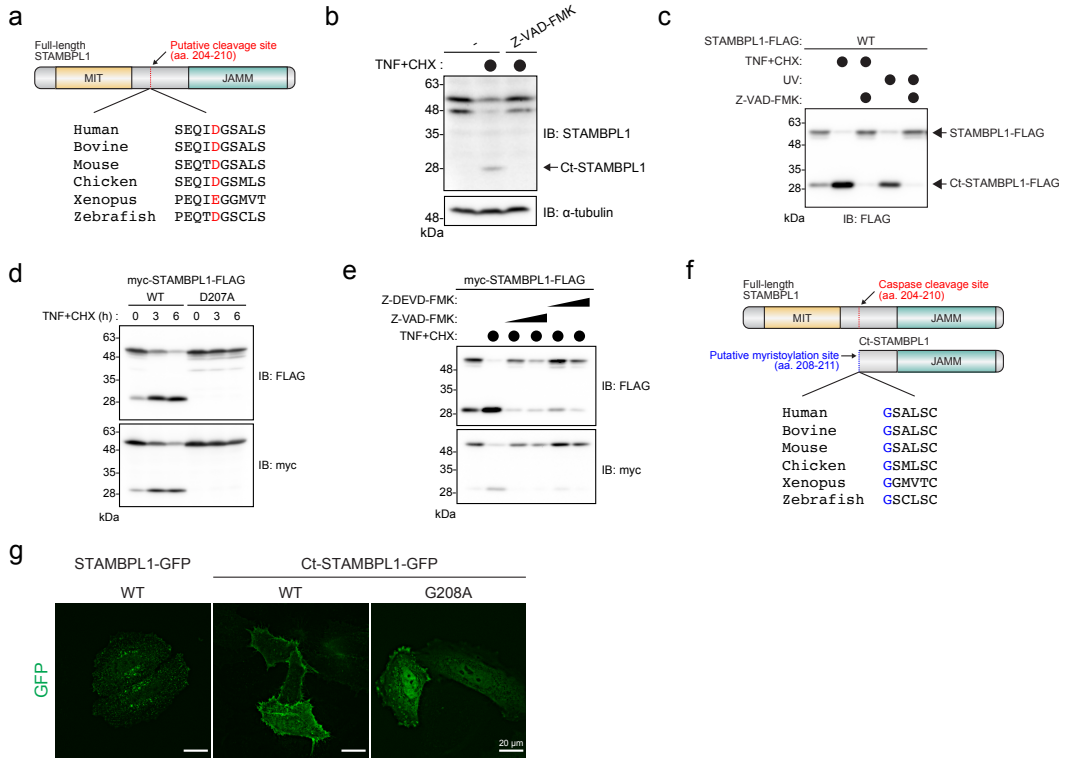

Fig. 11 STAMBPL1 cleavage by caspase-3 during apoptosis

a. Sequences showing a putative caspase-cleavage site in STAMBPL1 orthologs.

b. Endogenous STAMBPL1 cleavage upon induction of extrinsic apoptosis. HeLa cells were induced apoptosis using TNF and cycloheximide (CHX) in the presence of a pan-caspase inhibitor Z-VAD-FMK. The cells were lysed and subjected to immunoblotting.

c. STAMBPL1 cleavage upon induction of DNA damage-dependent intrinsic apoptosis. HeLa cells overexpressing FLAG-tagged STAMBPL1 were induced extrinsic or intrinsic apoptosis using TNF and CHX or ultraviolet radiation (UV), respectively, under treatment with or without Z-VAD-FMK and analyzed using similar method in b.

d. Effects of the mutation (D207A) in the caspase-cleavage site on the STAMBPL1 cleavage. HeLa cells overexpressing myc- and FLAG-tagged STAMBPL1 mutants were induced extrinsic apoptosis using TNF and CHX and analyzed using similar method in b.

e. Inhibition of STAMBPL1 cleavage during apoptosis using caspase-3 specific inhibitor Z-DEVD-FMK. HeLa cells overexpressing myc- and FLAG-tagged STAMBPL1 were induced extrinsic apoptosis using TNF and CHX in the presence of Z-VAD-FMK or Z-DEVD-FMK.

f. Sequences showing a putative myristoylation site in Ct-STAMBPL1 orthologs.

g. Cellular localization of Ct-STAMBPL1. HeLa cells overexpressing GFP-tagged STAMBPL1 mutants were analyzed using live-imaging observations. The single sections optimized by THUNDER Computational Clearing algorithm are shown.

Fig. 12

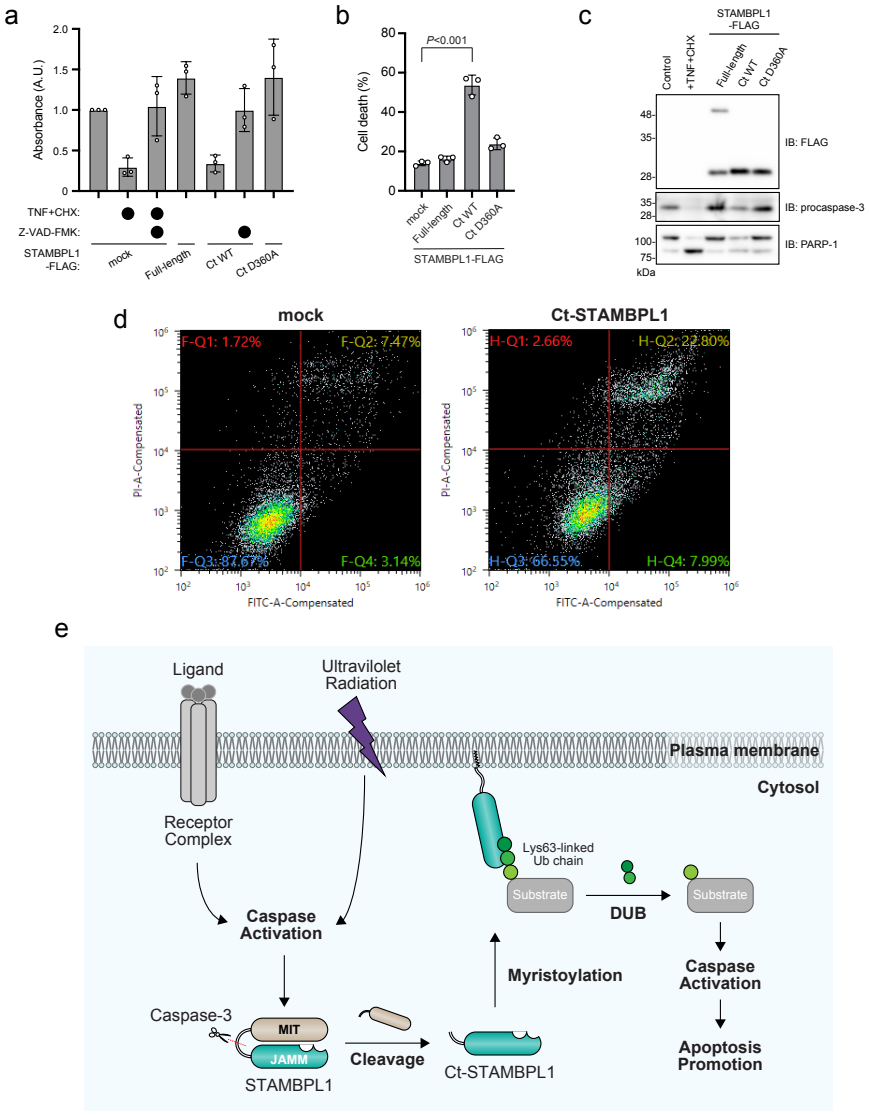

Fig. 12 Apoptosis induction by Ct-STAMBPL1 overexpression

a. Cell viability of HeLa cells overexpressing Ct-STAMBPL1. HeLa cells overexpressing FLAG-tagged STAMBPL1 mutants were subjected to WST-8 staining assay.

b. Cell death of HeLa cells overexpressing Ct-STAMBPL1. HeLa cells overexpressing FLAG-tagged STAMBPL1 mutants were subjected to SYTOX GREEN staining assay.

c. Effects of Ct-STAMBPL1 on caspase-3 and PARP-1 cleavages. HeLa cells overexpressing FLAG-tagged STAMBPL1 mutants were lysed and subjected to immunoblotting.

d. Effects of Ct-STAMBPL1 on cellular membrane flipping and permeabilization. HeLa cells overexpressing FLAG-tagged STAMBPL1 mutants were stained by propidium iodide and annexin V–fluorescein isothiocyanate (FITC) and analyzed using flow cytometry.

e. Working hypothesis of the STAMBPL1 autoinhibition and its role in apoptosis.

Fig. 13

a

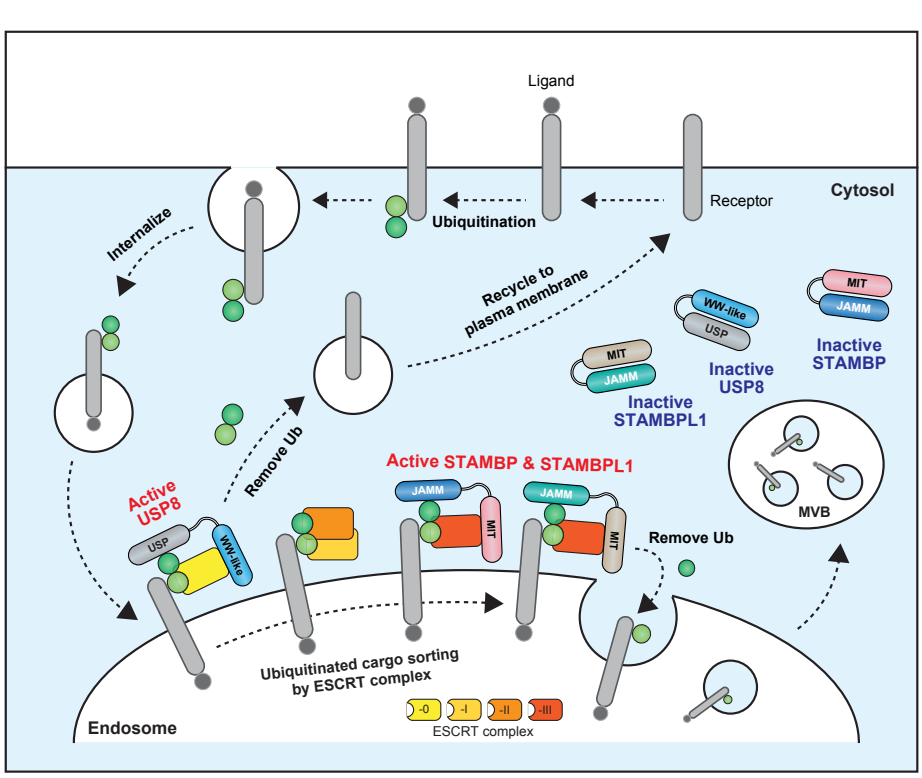

Fig. 13 *Cis*-regulations of endosomal DUBs and its roles in endocytosis

a. Working hypothesis of endosomal DUBs role in endocytosis. Deubiquitination of ubiquitinated membrane receptors at the early and late endosomes is involved in their recycling to the plasma membrane and lysosomal degradation, respectively. USP8, STAMBP, and STAMBPL1 (STAMBPs) are the responsible DUBs for these regulations. Most of them are autoinhibited with the closed conformation in the cytosol. On the other hand, USP8 and STAMBPs are activated at the endosome through their interactions with appropriate partners in ESCRT complex. I provide an attractive model that, upon binding to ESCRT proteins, USP8 and STAMBPs are relieved from autoinhibition, thereby activating in a site-specific manner.